AD-A105 067 CINCINNATI UNIV OH SOLID STATE ELECTRONICS LAB F/G 20/12
INTEGRATION OF A DETECTOR ARRAY WITH AN OPTICAL WAVEGUIDE STRUC--ETC(U)
AUG 81 J T BOYD, D A RAMEY, C L CHEN AFOSR-76-3032
UNCLASSIFIED AFOSR-TR-81-0695 NL

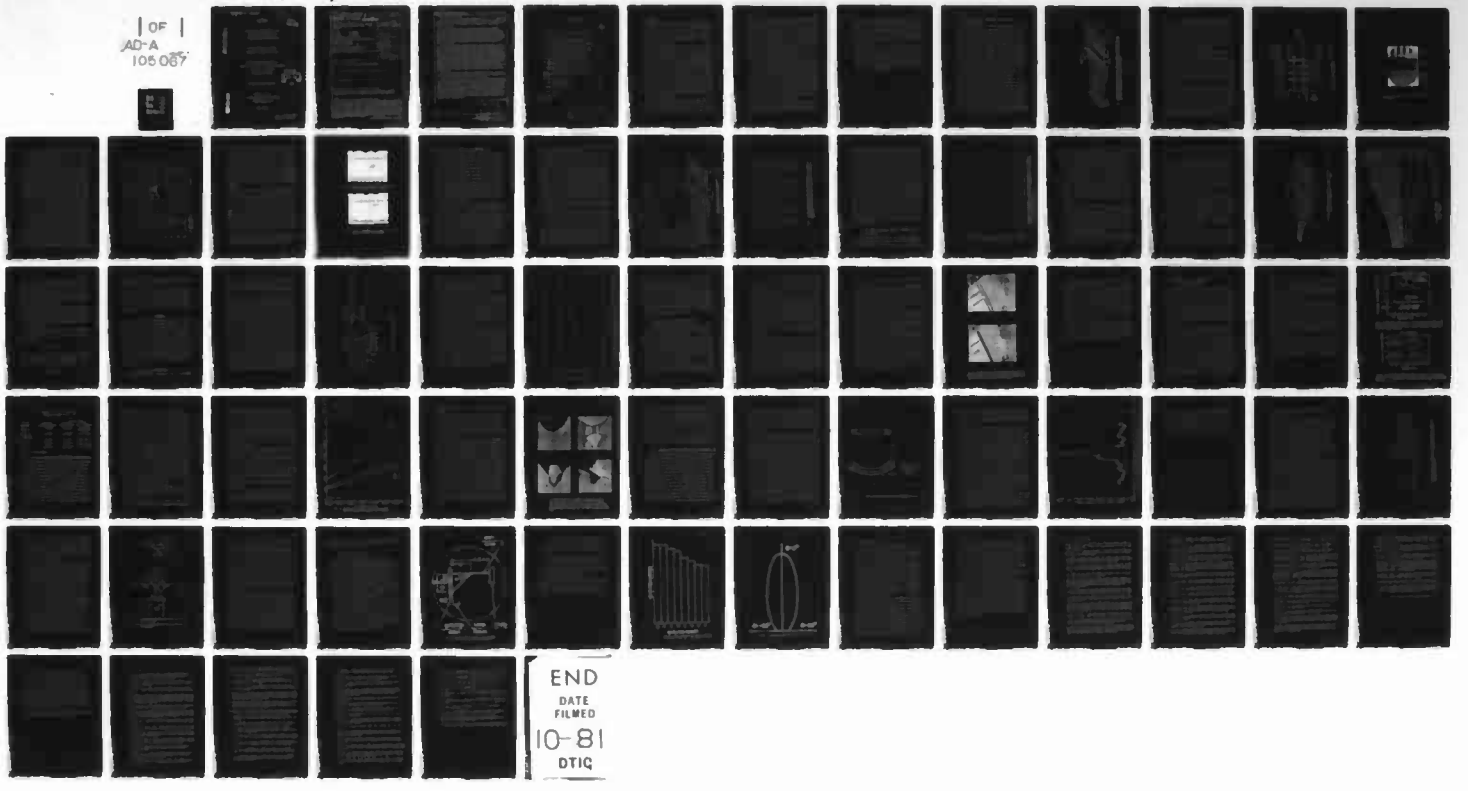

END
DATE FILMED
10-81
DTIC

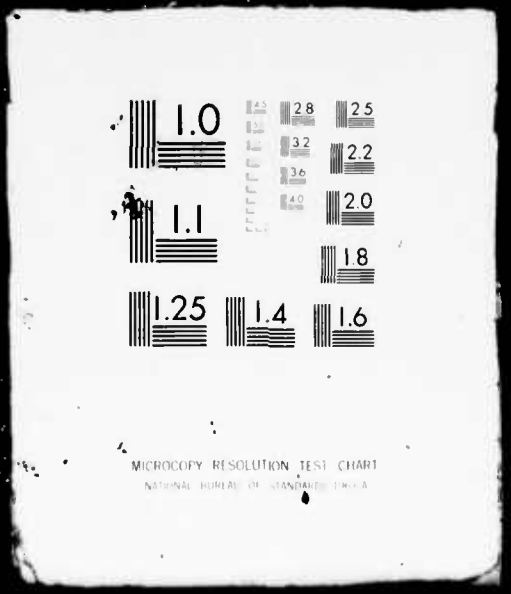

Final Report
15 Jun 76-14 Mar 81

INTEGRATION OF A DETECTOR ARRAY WITH AN OPTICAL WAVEGUIDE STRUCTURE AND APPLICATIONS TO SIGNAL PROCESSING

J.T. Boyd, D.A. Ramey, C.L. Chen
A. Naumaan, S. Dutta, and S.H. Chang

Solid State Electronics Laboratory
Department of Electrical and Computer Engineering
Univerisity of Cincinnati
Cincinnati, Ohio 45221

J.T. Boyd, Principal Investigator

Prepared for the:
Air Force Office of Scientific Research
Grant AFOSR-76-3032

Aug. 7, 1981

Unclassified

SECURITY CLASSIFICATION OF THIS PAGE (When Data Entered)

REPORT DOCUMENTATION PAGE	READ INSTRUCTIONS BEFORE COMPLETING FORM
1. REPORT NUMBER: AFOSR-TR- 81 -0695	2. GOVT ACCESSION NO.: AD-A105067	3. RECIPIENT'S CATALOG NUMBER
4. TITLE (and Subtitle): Integration of a Detector Array with an Optical Waveguide Structure and Applications to Signal Processing	5. TYPE OF REPORT & PERIOD COVERED: Final Technical Report 15 June 1976 - 14 March 1981
	6. PERFORMING ORG. REPORT NUMBER
7. AUTHOR(s): J.T. Boyd, D.A. Ramey, C.L. Chen, A. Naumaan, S. Dutta, S.H. Chang	8. CONTRACT OR GRANT NUMBER(s): AFOSR-76-3032
9. PERFORMING ORGANIZATION NAME AND ADDRESS: Department of Electrical & Computer Engineering, University of Cincinnati, Cincinnati, Ohio 45221	10. PROGRAM ELEMENT, PROJECT, TASK AREA & WORK UNIT NUMBERS: 61102F, 2305/B1
11. CONTROLLING OFFICE NAME AND ADDRESS: Air Force Office of Scientific Research, Bolling Air Force Base, DC 20332	12. REPORT DATE: August 7, 1981
	13. NUMBER OF PAGES: 69
14. MONITORING AGENCY NAME & ADDRESS (if different from Controlling Office)	15. SECURITY CLASS. (of this report): Unclassified
	15A. DECLASSIFICATION/DOWNGRADING SCHEDULE: None

16. DISTRIBUTION STATEMENT (of this Report)

Approved for public release; distribution unlimited.

17. DISTRIBUTION STATEMENT (of the abstract entered in Block 20, if different from Report)

18. SUPPLEMENTARY NOTES

19. KEY WORDS (Continue on reverse side if necessary and identify by block number)

Integrated optics, charge coupled devices, optical waveguide, spectrum analysis, transversal filter, phosphosilicate glass, laser annealing.

20. ABSTRACT (Continue on reverse side if necessary and identify by block number)

Both planar thin film and channel optical waveguides have been integrated with charge-coupled devices (CCDs). Coupling of light from the waveguide region to the detector elements utilizes a smooth and uniformly-tapered region of SiO_2 to minimize scattering. CCD transfer inefficiency of 1.0×10^{-4} is consistently obtained for a number of devices. A channel waveguide array formed in a fan-out pattern is introduced as a means of enhancing focal plane resolution in integrated optical devices using optical waveguide lenses. High spatial resolution can thus be obtained without making detector spacings too small, thus avoiding

DD FORM 1 JAN 73 1473 EDITION OF 1 NOV 65 IS OBSOLETE

Unclassified

SECURITY CLASSIFICATION OF THIS PAGE (When Data Entered)

detector problems with regard to fabrication, crosstalk, linearity, and charge transfer inefficiency.

Operation of an integrated optical channel waveguide array-CCD transversal filter is reported. Channel waveguides formed in V-grooves couple directly to the sensor elements of the four phase, double polysilicon CCD. Experimental results include a filter transfer function having good agreement with theoretical results.

The voltage contrast mode of a scanning electron microscope (SEM) is utilized to observe charge-coupled devices (CCDs) which have been cross sectioned. A new cross sectioning technique which uses anisotropic etching to accurately define the axis along which fracture occurs is presented. Lapping is not required in this technique, as smooth surfaces result from the controlled fracturing. SEM imaging of the region just beneath a CCD double-level, polycrystalline silicon electrode structure revealed a region of contrast which appeared and disappeared under the presence and absence of an applied pulsed bias.

We have achieved the first demonstration of laser annealing of thin-film optical waveguides to reduce scattering losses. Values of waveguide loss as low as .01 dB/cm have been measured for laser-annealed ZnO waveguides and for Corning 7059 glass waveguides which have been both laser annealed and had surface coatings applied. Significant improvements have also been observed for Si_3N_4, Nb_2O_5, and Ta_2O_5 waveguides. A 50W CO_2 laser for laser annealing along with a beam scanner and a focusing lens were used. Precise measurements of waveguide loss were performed by sampling a streak of light propagating in a thin-film waveguide with a fiber probe incorporated into a scanning photometric microscope as a function of distance along the propagation axis. The presence of the microscope allowed precise positioning of the fiber with respect to the waveguide and motorized scanning of the fiber transverse to the propagation axis. Electronic signal averaging during this scan including correction for laser power fluctuations was used to improve the precision of the measurement.

An extensive analysis of crosstalk in photodetector arrays is described. The effect of a lens imaging a field distribution onto the photodetector array is included along with the effects of carrier diffusion.

We have carried out an investigation of the use of phosphosilicate glass (PSG) flow for integrated optical circuits. PSG layers of thicknesses ranging from 4 to 22 μm were chemically vapor deposited on V-grooves in silicon substrates having a depth of 175 μm. The effect on the flow of (1) P_2O_5 concentration in PSG layers (5-10 mol%), (2) ambient during flow (dry O_2, wet O_2, $POCl_3$, and wet N_2), (3) temperature (1000°-1200°C) and (4) time (30-120 min) of the process has been determined. The extent of flow, as measured by curvature of the rounded corners, has been plotted against PSG layer thickness and reflow time. Radii of curvature up to 36 μm through 70° bends have been measured. Flow of PSG is used along with anisotropic etching to form a novel optical waveguide lens.

Table of Contents

I. Introduction

The present report describes the accomplishments of research involving integration of a photodetector array with an optical waveguide structure and applications to signal processing. Most of the important results have been published (see Section VI for a list of program publications) so the present report will not contain full details of all accomplishments. For those wishing more detail in a certain area, specific publications will be referenced where more details appear.

Major research accomplishments occurred in three areas: (1) Improvements in materials for integrated optics, (2) Various devices using an array of channel waveguides coupled to a linear charge-coupled device (CCD) imaging array, and (3) Planar waveguides coupled to integrated photodetectors. Noteworthy in the first area is the achievement of values of planar waveguide propagation loss (.01 dB/cm) an order of magnitude better than any value ever reported previously. We accomplished this for two different materials by laser annealing: Corning 7059 glass and zinc oxide.[1, 2] Major accomplishments in the second area include experimental demonstration of an integrated channel waveguide - CCD transversal filter,[3] of a channel waveguide fan-out array coupled to a CCD for high resolution imaging[4] and an analysis of cross-talk in photodetector arrays.[5] Of note in the third area was the first demonstration of an optical waveguide coupled to a CCD,[6, 7], formation of taper couplers for these devices,[8] and the use of these device structures for performing scattering measurements.[9]

The present research program has thus far investigated a number of integrated optical device configurations utilizing a silicon substrate. The motivation for investigating devices utilizing silicon is first, due to its potential use for such signal processing devices as the integrated optical

spectrum analyzer,[10-13] second, its usefulness for performing waveguide detection in such signal processing devices formed on $LiNbO_3$, third, to provide integration of external components in fiber optic interferometric devices,[14] and fourth, to allow combination of integrated optical devices and integrated electronic circuits to form higher data rate systems. The recent demonstration in our laboratory of waveguide loss in thin film waveguides as low as .01 dB/cm after laser annealing implies that it may be worthwhile considering formation of the interferometer in an optical waveguide rather than a fiber.[14] Such a configuration would significantly reduce the size and allow total component integration on a silicon wafer substrate. This reduction in size and increase in component integration would be very desirable for application of guided wave interferometric sensors in military systems.

Many of the device configurations considered in the present program have involved the integration of optical channel waveguide arrays integrated with CCDs. In addition to research described here, we have demonstrated the coupling of optical fibers to such channel waveguides under sponsorship of NSF.[15] Channel waveguides provide confinement of the propagating field in all transverse directions. When an array of channel waveguides is integrated with a CCD, each channel waveguide terminates onto a linear CCD imager array element. The CCD then multiplexes or combines in a prescribed manner the information contained in the parallel optical channels, providing a serial electrical output. Transversal filtering in this manner has been demonstrated as a part of the present research program.[3] Examples of several other ways this can be used advantageously are described throughout this report.

The effect of waveguide scattering on the integrated optical signal processing device dynamic range has been analyzed and numerical results presented for variations in the scattering pattern as a part of the present

research program.[16] The results of this analysis indicate that dynamic range is degraded in proportion to waveguide scattering in such a way that a reduction in waveguide attenuation due to scattering by a factor of 10 leads to a reduction in dynamic range of about 10 dB and conversely. Thus, the fact that we have reduced scattering in several optical waveguide materials by factors of 100 over values previously reported in the literature implies that devices which could use these materials could achieve a significant increase in dynamic range.

In what follows we first discuss in II channel waveguide arrays coupled to integrated CCDs which have been investigated. In this section we also discuss the first use of voltage contrast in a scanning electron microscope to image a CCD during operation.[17] We then consider material improvements for integrated optics in III and the coupling of planar waveguides to photoelector arrays in IV. We follow this with conclusions in V, a list of program publications in VI, and finally with acknowledgements and references.

II. Array of Channel Waveguides Coupled to An Integrated CCD

A. Device Structure

As noted in the introduction, an optical channel waveguide array coupled to a CCD linear imaging array and integrated onto the same silicon substrate was fabricated and successfully operated early in the program.[18, 19] This device is shown schematically in Fig. 1. The channel waveguide array is formed by preferential-etching of V-grooves in the 100 plane of silicon.[20, 21] This integrated device differs from planar slab waveguide CCD structures in that the present structure is configured such that an individual channel waveguide is coupled to each array element of the CCD image sensor. This integrated device structure thus provides a method for the parallel injection of signals into a CCD with a high degree of isolation between parallel channels. Channel isolation and channel density are expected to be superior to that of parallel electrical signal injection because of the absence of capacitive coupling in the former. Furthermore, because light propagating in each channel waveguide is bound to this region, better channel isolation than would exist in a comparable bulk optical wave structure[22] is expected.

Details of the fabrication of this device have been published elsewhere.[19] A novel aspect of this devise is the CCD photodiode coupling structure. The realization of this device depends on a good coupling structure between the photodiode array and the CCD. The signal injection from the photodiode array into the CCD and the emergence of the signal from the CCD forms a parallel-in/serial-out conversion. The coupling structure should provide an isolated channel for each photodiode to transfer signal into the corresponding CCD cell. A new coupling structure which does not complicate the CCD structure and which is compatible with relaxed photolithographic tolerances has been used. In this structure very small contact holes are not

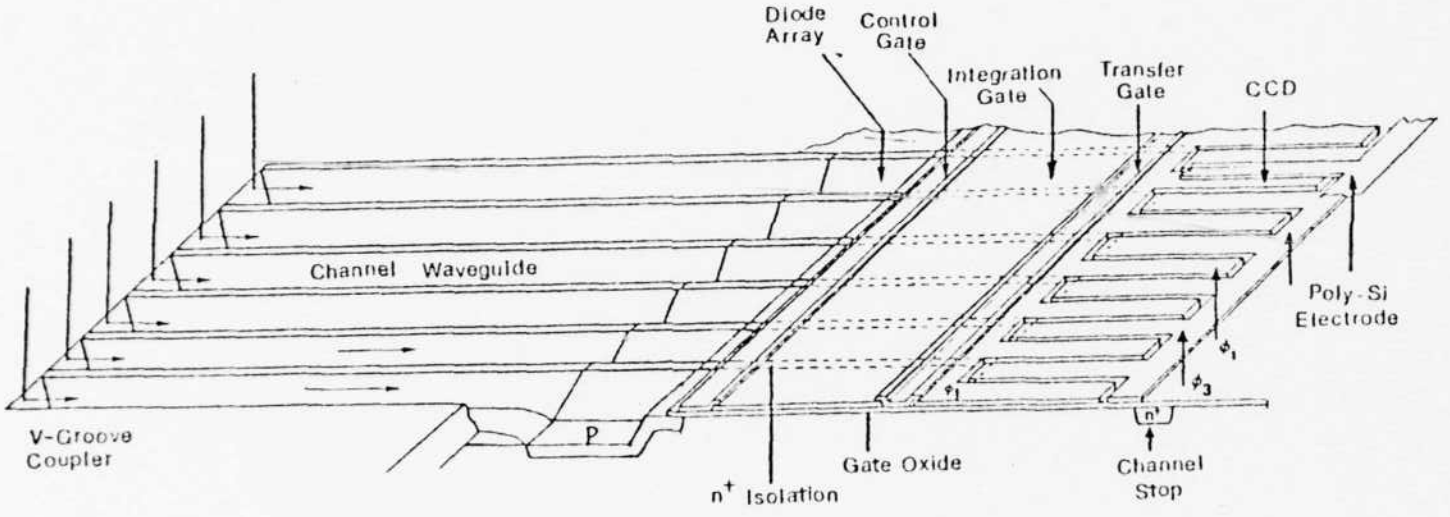

Fig. 1 Channel optical waveguide imager. Channel waveguides are coupled to a four-phase, double polysilicon PA-CCD device with a V-groove end coupler for laser light coupling into channel waveguides.

needed on the rather narrow polysilicon bus electrodes which connect all the electrodes of each phase to the same side of the CCD. In this design, one of the CCD phases for a two phase device and two of the phases for a four phase device are placed on the photodiode side of the CCD. These bus electrodes also serve as a part of the coupling structure between the photodiode array and the CCD. Since the bus lines can be placed on both sides of the CCD, conventional CCD device design can be used except with a modification on the channel stop diffusion under the phase one bus line. The usual MOS channel should be left here to allow charge transfer into the CCD.

Figure 2 shows the coupling structure of a photodiode array with a four phase, double polysilicon CCD. The coupling structure consists of three MOS gates in series. These are the bias gate (BG), carrier integration gate (CIG) and transfer gate (TG). Underneath these gates, a series of parallel n^+ diffusion bars extending from the edge of the V-grooves isolating the photodiodes through the $\emptyset_1$ bus line and stopping under the phase three bus line of the CCD forms potential barriers to create electrically isolated coupling channels to exist from the photodiode to the CCD. This kind of a coupling structure provides for signal integration capability for low level light operation.

Figure 3 shows the coupling structure of a fabricated photodiode array-CCD imager. A four-phase CCD is used in this particular process, and V-groove isolation diffusion is used between photodiodes. In this device, the bias gate is 7.5 μm wide with 2.5 μm overlap of the photodiode and integration gate. The transfer gate is the same size as the bias gate with 2.5 μm overlap of the integration gate and of the CCD phase one bus line. The size of the integration gate is chosen to have nearly the same area as one of the CCD electrodes to ensure charge overflow does not occur inside the CCD when a large charge packet is transferred from the integration gate. The integration

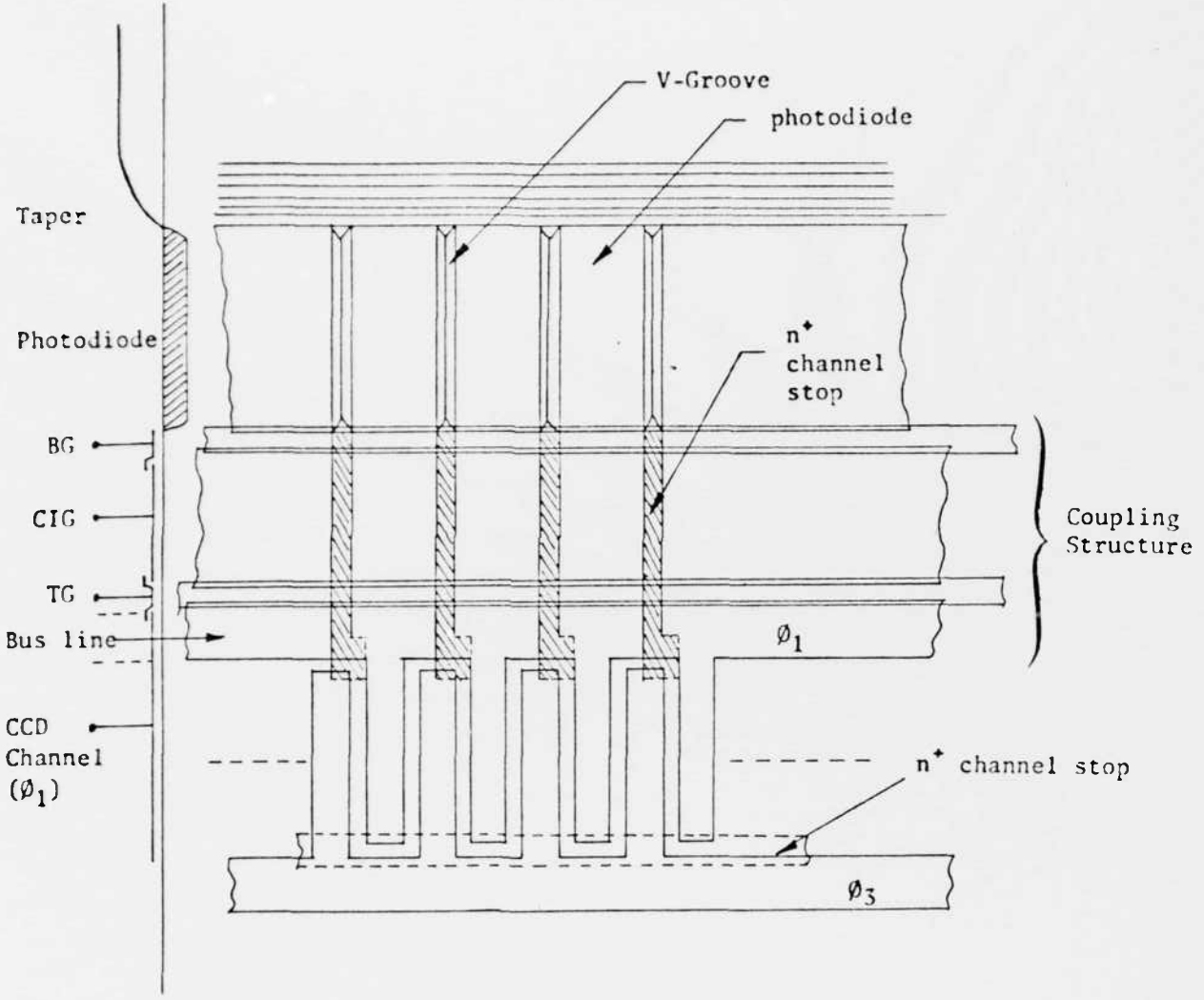

Fig. 2 Coupling structure between a photodiode array and a four phase CCD with cross section diagram at the left.

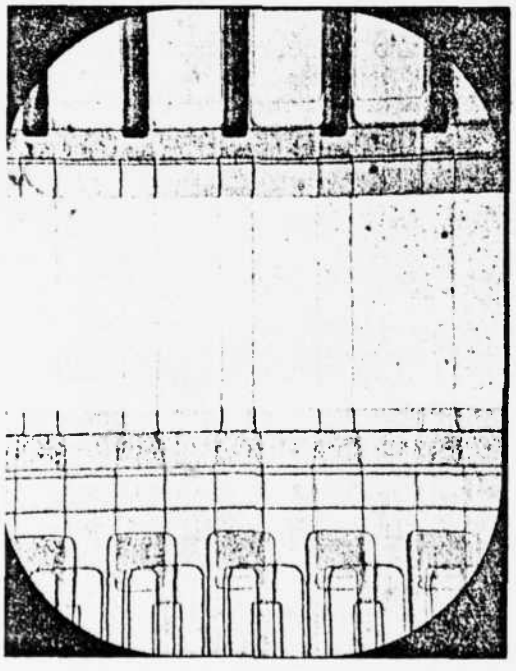

Fig. 3 Coupling structure of a four-phase, double polysilicon photodiode CCD device.

gate is 25 μm wide and 62.5 μm long in this device. Notice that the n^+ channel isolation diffusion extends across the CCD ϕ_1 bus line and terminates at the edge of the ϕ_3 electrode. This arrangement ensures isolation of the CCD cell, and maintains charge shifting directionality.

The dynamic behavior of the 4 phase CCD is controlled by the 4 phase clock voltage waveforms as well as the voltage waveforms which control parallel injection and the output amplifier. The timing diagram of these voltage waveforms is shown in Fig. 4. The p channel CCD clock voltage waveforms are 90 degreee phase shifted to adjacent phases such that ϕ_1 and ϕ_3 are complementary waveforms, as are those of ϕ_2 and ϕ_4. The input gate pulse is synchronized with the negative going edge of the ϕ_1 pulse and the same for the reset gate pulse since the first and last CCD electrodes are designed to be ϕ_1 electrodes. A sampling pulse is synchronized with the negative going edge of the ϕ_4 pulse. The timing sequence of the output circuit is as follows. During the period ϕ_1 is negative the last CCD electrode is receiving charge, the reset pulse having already allowed the reference voltage to be reset at the output. The occurrance of reset of the output during the early part of the period when ϕ_1 is negative provides a longer available reset time which could last as long as half of a clock cycle. After reset the ϕ_1 clock turns off its respective electrodes and forces charge through the channel beneath the dc biased output gate toward the output diode. The sampling pulse is turned on late during the period when the ϕ_1 electrodes are turned off so as to provide a longer charge transfer time. Since the sampling circuit required only a short sampling time in comparison to the reset time, the width of the sampling pulse can be adjusted as small as possible. Also shown in Fig. 4 are the transfer gate and charge integration gate pulses for device operation.

To evaluate the performance of the CCD, the most important parameter characterizing operation is the charge transfer efficiency or, equivalently,

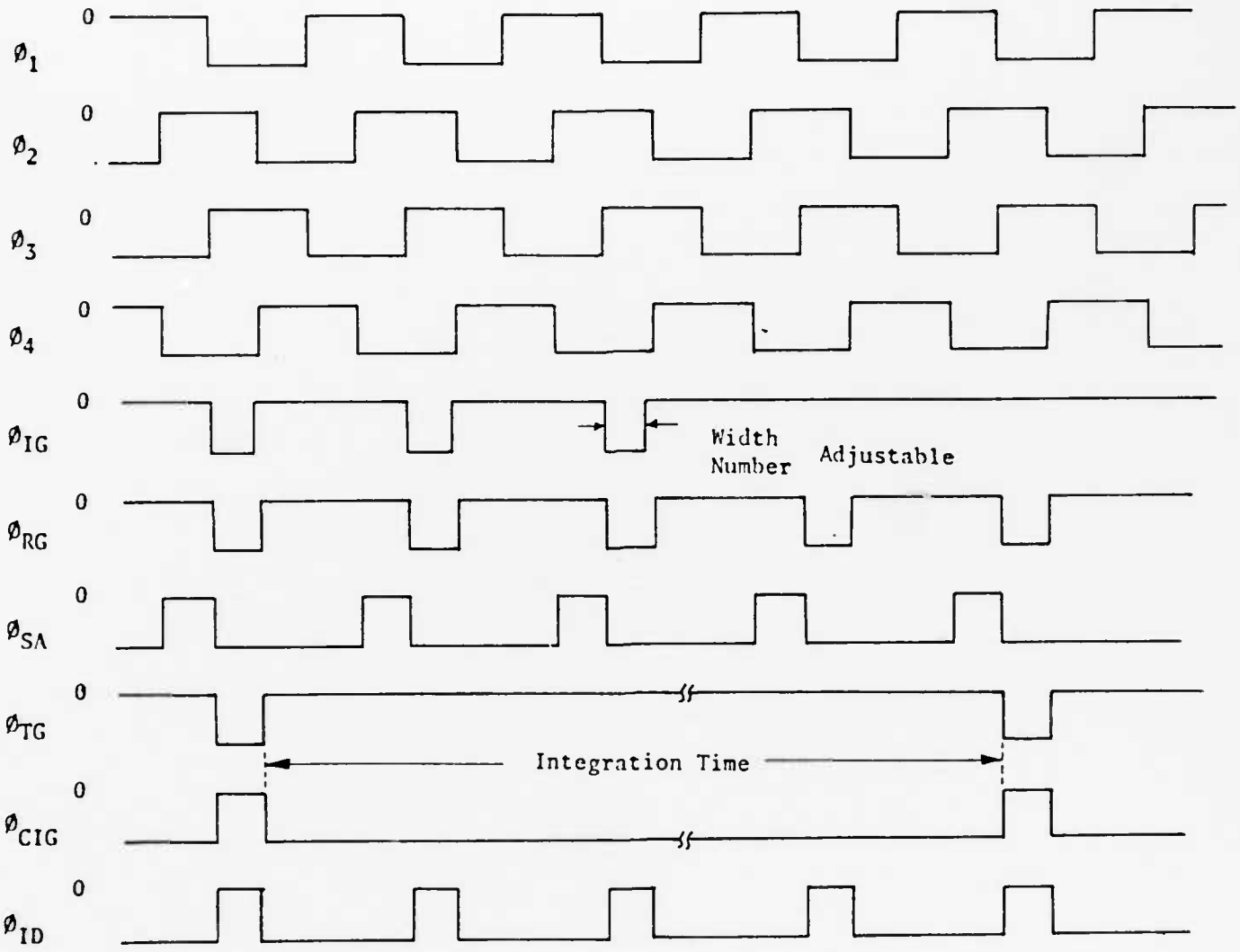

Fig. 4 Clock waveform and timing diagram for a four-phase, photodiode array-CCD device operation.

transfer inefficiency which is one minus transfer efficiency. Transfer inefficiency measures the fraction of charge left behind upon each transfer. Transfer inefficiency can be determined by first operating a CCD without any input signal for a certain period of time such that all the trapped charge in surface states is released. If a signal charge packet is then injected into the CCD, many of the carriers in this packet are trapped. Subsequent injected pulses do not encounter as many empty traps. Since the traps release trapped signal charge at later times, the output of the CCD will be a dispersed pulse train. Figure 5-a illustrates CCD response to a train of 7 equal amplitude input pulses. Note that the amplitude of the first pulse is degraded and residual pulses follow the seven output pulses, in accordance with the above explanation.

The degree of signal charge spreading is characterized by the charge transfer inefficiency. Charge transfer inefficiency can be calculated from the CCD response to an equal amplitude pulse train.[23] As shown in Fig. 5-a the discrepancy of the first output pulse amplitudes shows loss of signal charge, while the small amplitude pulses following the last signal pulse correspond to the emission of trapped signal charge. The presence of bias charge injected into the CCD at all times significantly reduces the above problem by keeping the surface traps filled. Transfer inefficiency improves significantly as a result and the associate signal distortion is eliminated, as is indicated in Fig. 5-b which corresponds to the situation in Fig. 5-a but with bias charge. Using the established procedure to determine transfer inefficiency,[23] the transfer inefficiency of the device tested in Fig. 12 is $1.0 \times 10.^{-4}$

Experimental measurements of the optical response of this device have been published elsewhere[19] and thus will not be repeated here. Further experimental results will be discussed in later sections of this chapter.

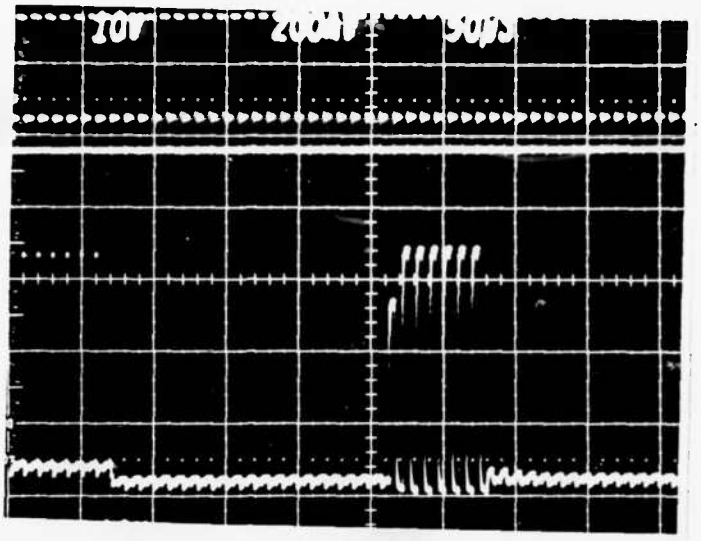

Fig. 5(a) Output of a four-phase, double polysilicon CCD clocked at 100 KHz without bias charge.

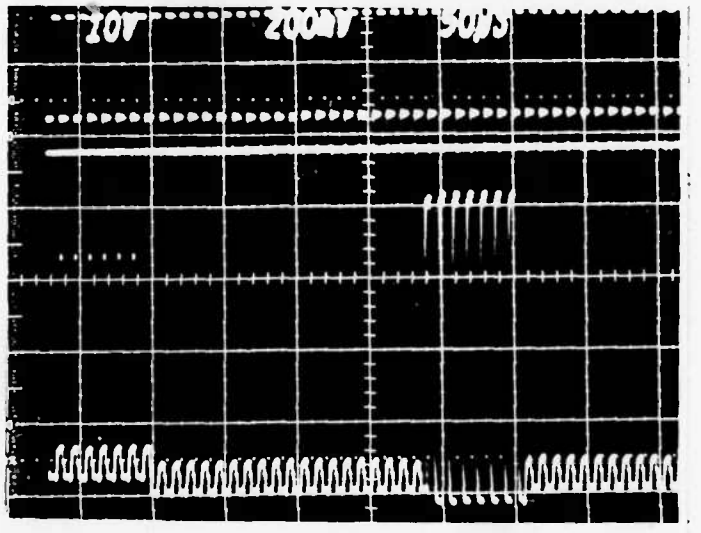

Fig. 5(b) Output of the above CCD with about 6% bias charge. Transfer efficiency is about 0.9999.

B. Integrated Channel Waveguide - CCD Transversal Filter

Operation of an array of optical channel waveguides integrated with a charge-coupled device (CCD) as a transversal filter is reported in this section. The presence of channels having low loss and good isolation presents excellent potential for applications such as multiplexing or transversal filtering in which optical channels can replace electrical channels and thereby realize many of the same advantages that result from the use of optical fibers in various applications. Light propagating in each element of the channel waveguide array is coupled to a sensor element of the CCD efficiently and with minimal scatter.[8] The CCD is operated in such a manner so that these inputs are summed together with appropriate delay. Transversal filtering then results since a delay line with parallel weighted input and serial output has the same impulse response and transfer function as the same delay line with serial input and parallel weighted output, the configuration used to implement conventional CCD transversal filters.[24]

Optical transversal filtering with CCDs has been demonstrated previously by illuminating a CCD linear imager through a mask which incorporates the weighting.[22] However, the use of channel waveguides for confining the light has potential for more accurate control of channel weighting since geometrical access to each channel is available, much greater channel isolation, and, because of the simplicity of the channel waveguide structure offers potential for very high channel densities. In addition, input of light to each channel through an optical fiber is a distinct possibility, since direct coupling of light from fibers to channel waveguides of the type present in the device being reported herein has previously been demonstrated.[15] A high speed programmable capability could be otained by pulse duration modulation or by direct modulation of a semiconductor laser array. The demonstration of the

mounting of semiconouctor laser array onto silicon[25] implies that a compact hybrid device structure is a realistic possibility.

The configuration of the channel waveguide array-CCD transversal filter is shown schematically in Figure 6-a. Channel waveguides ano the CCD are formeo as in the device described in the previous reaction. As each channel waveguide terminates into a separate sensor region, as shown in Fig. 6-a, a large portion of the light incident on this termination excites carriers which are collected under the integration gate as the potentials of the control and integration gates are suitably adjusted. At the end of each clock period, the transfer gate is turned on, as shown in the timing diagram shown in Fig. 6-b, so that the collected charge is transferred into the CCD. This charge transfer occurs simultaneously for each array element and in a time much less than 1/4 of the CCD clock period. Once this charge has tranferred into the CCD, the transfer gate is turned off and the charge is shifted along the CCD. Clocking in this manner performs the delay and summing function characteristic of a transversal filter. The four MOS transistors at the input to the LED array are included to symbolize analog multiplication for establishing tap weights in the transversal filter.

The device in Fig. 6 has been fabricated. The 20 channel waveguides are each 25 μm by 1.6 mm with a periodic spacing of 35 μm. The diffused portion of the sensor elements is 25 μm by 114 μm with 90% of this area overlapping down into the V-groove and the integration gate is 25 μm by 100 μm, both having a periodic spacing of 35 m. The CCD polysilicon electrodes are 15 μm by 130 μm for the first level and 12.5 μm x 130 μm for the second overlapping level. An MOS reset amplifier with employs a double reset gate with the gate closest to the floating diffusion held at dc and the other pulsed is integrated at the CCD output, as this arrangement reduces clock feedthrough. CCD charge transfer inefficiency, defineo as the fraction of charge lost per

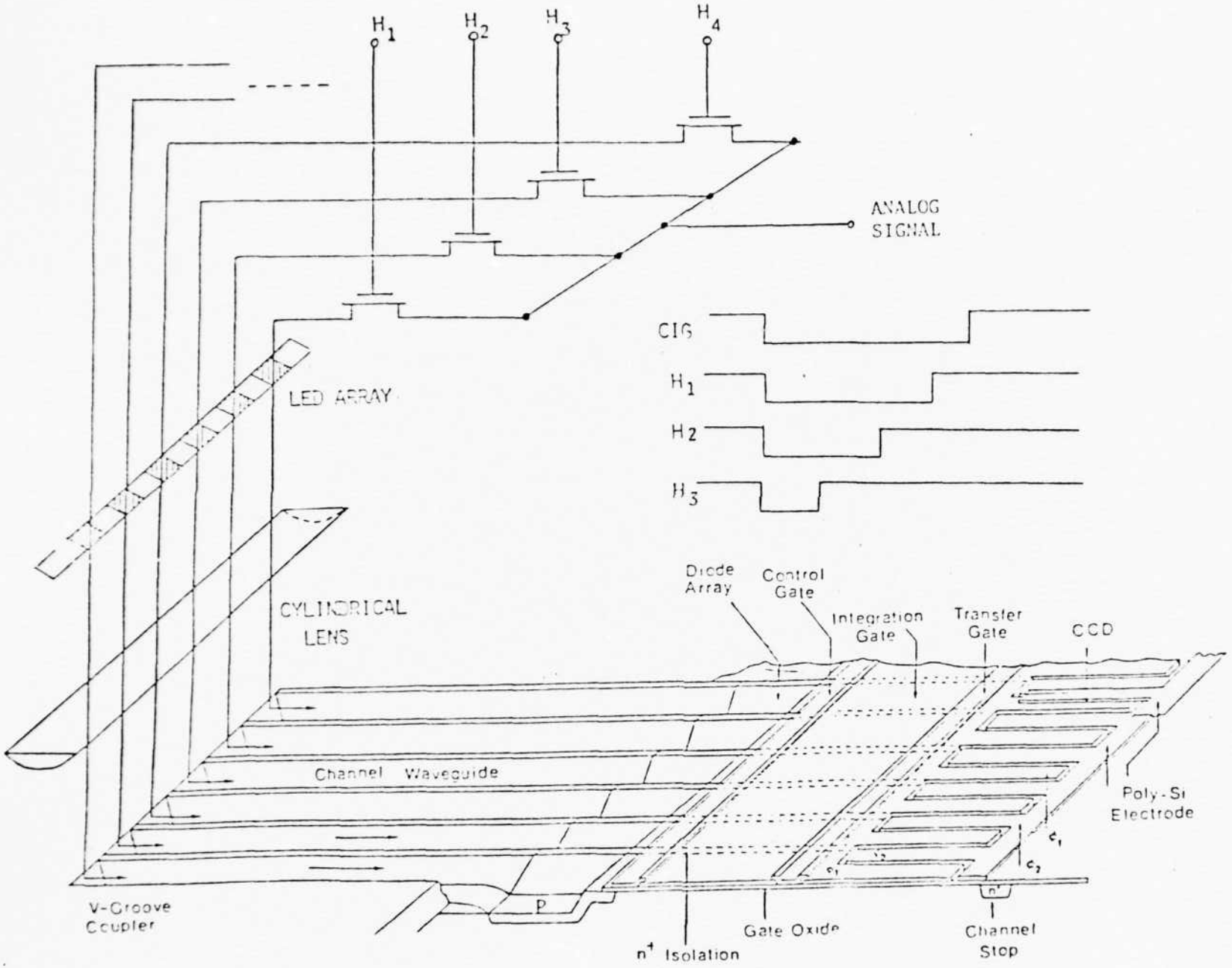

Fig. 6(a) Device configuration of the integrated optical channel waveguide-CCD transversal filter.

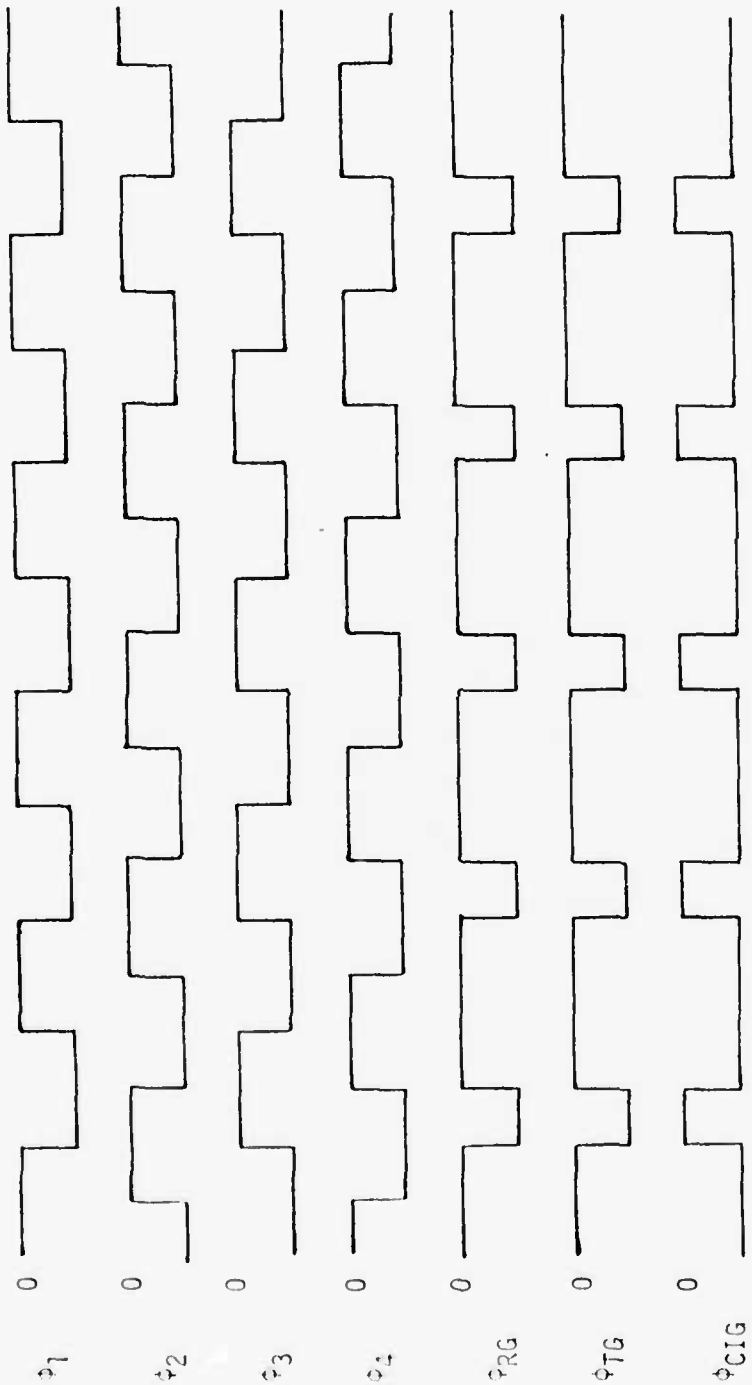

Fig. 6(b) Timing diagram for operation of the device shown in (a) showing voltage variations with time for the four phases, the reset gate (RG), the transfer gate (TG), and the carrier integration gate (CIG).

transfer, is measured by applying a small group of electrical pulses to the serial input preceeded by a long period of no input, as discussed earlier. A transfer inefficiency of 1.0×10^{-4} has been measured for this device also.

The device in Fig. 6 has been excited optical by utilizing V-groove end-coupling for coupling light into the channel waveguides. This coupling mehod utilizes the fact that V-grooves in silicon have V surfaces at their terminations. By depositing aluminum over these end surfaces, a mirror is formed which allows light to be reflected directly into the waveguide.

Operation of the above device as a tranversal filter has been achieved by foucusing light from a single light-emitting diode (LED) with a cylindrical lens onto the end-coupling region. Use of single LED does not allow the flexibility of varying the tap weighting as use of an array would, but it does allow demonstration of transversal filter operation for fixed and uniform tap weighting. By making the focal region longer than the end coupler region, we expect that the light intensity distribution along the end coupler is nearly uniform so that the effective tap weighting is nearly uniform. To measure the filter transfer function of frequency. Fig. 7 shows a plot of the measured and theoretical transfer function of such a filter for a 20 tap device having equal tap weighting. Note that the level of the experimentally-measured sidelobes is slightly less than that of the theoretical value. We attribute this to inherent apodization present in the distribution of the incident light focused onto the end-coupler region.

C. Fan-Out Channel Waveguide Array For High Resolution Optical Waveguide Imaging

Signal processing devices such as the integrated optical spectrum analyzer[10-12] are motivating the development of integrated optical waveguide lenses.[27-30] The constraints of limited substrate area and high frequency resolu-

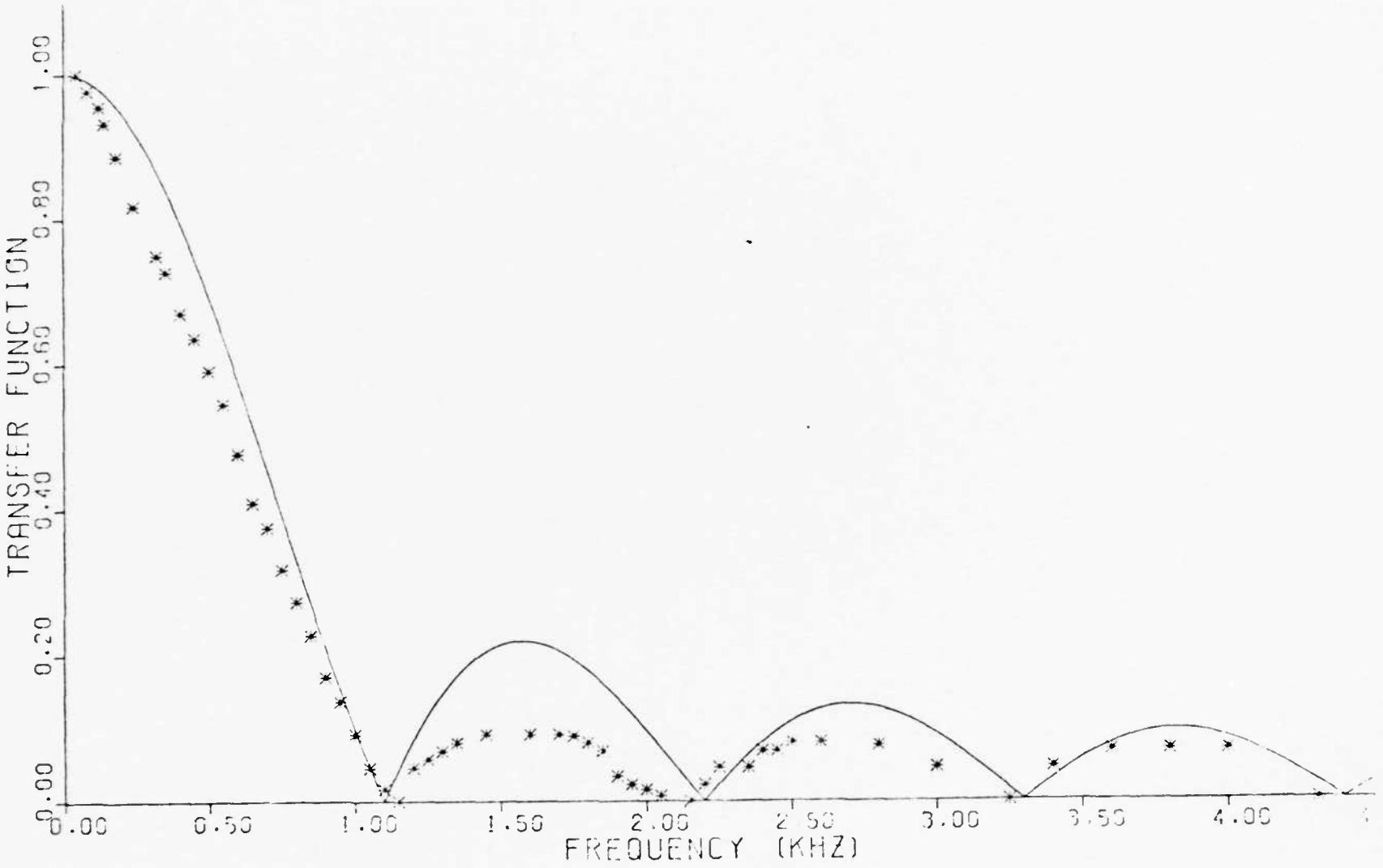

Fig. 7 Theoretical and experimental values of the transfer function as a function of frequency for the integrated optical channel waveguide array-CCD transversal filter. The solid line corresponds to the theoretical value, while the points correspond to experimental values.

tion lead to the use of small f-number waveguide lenses. To fully resolve focal plane light distributions for such lenses, detector arrays having center-to-center spacings of a few microns are required. As system requirements point toward several hundred resolvable spots, use of a CCD linear imaging array is advantageous. Forming a CCD linear image array having a period of several microns is difficult but possible. However, as integrated optical devices such as the spectrum analyzer are expected to use a semiconductor laser having λ = .82 μm, the absorption length in silicon is about 15 μm.[5] The fabrication of a CCD linear imaging array having a period significantly less than the absorption length, but in which channel isolation is to be maintained, adds considerable difficulty to the design and fabrication tasks. For these reasons we are presenting an alternate approach utilizing a channel waveguide fan-out array coupled to an integrated CCD. This device provides the desired fine spatial resolution, while allowing use of a CCD having a much larger period. The larger period simplifies CCD fabrication and provides improved channel isolation.

Implementation of the integrated optical devices is currently being investigated using both $LiNbO_3$ and silicon substrates. $LiNbO_3$ structures provide superior acousto-optic performance, while silicon structures provide for integration of detectors and more economical processing and material costs. The fan-out channel waveguide array described herein is fabricated on a silicon substrate, thus being directly applicable to integrated optical silicon devices. However, the concept is applicable $LiNbO_3$ devices, and would provide many of the same advantages as noted above.

To fabricate the devices described herein, a new procedure in polyurethane waveguide fabrication technology has been developed and is reported. For the first time, high quality patterns having 5 micron resolution in poly-

urethane films can be formed, using a minimum of equipment and processing steps.

The fan-out channel waveguide array coupled to a CCD is shown in Fig. 8-a. The fan-out array performs several functions simultaneously. Coupling between the slab waveguide and separate, independent channel waveguides effects a high resolution spatial sampling function. Since the slab and channel waveguides are formed simultaneously, the thickness of both the slab and channel waveguides are essentially the same so that scattering due to the resulting mode structure difference is minimized.[32] High spatial resolution is obtained since the input center-to-center spacing of the fan array is considerably less than the actual center-to-center spacing of the detector array. The increase in spatial resolution results without any sacrifice in detector array performance with regard to crosstalk.

To achieve the needed guiding layer structure, the polyurethane is deposited by spinning it over thermally-grown SiO_2, which has a lower index of refraction. The SiO_2 must be somewhat greater than a wavelength in thickness to prevent tunnelling through to the high index silicon substrate.[33] This is a commonly accepted waveguide configuration for integrated optics. Any substrate can be used for polyurethane waveguides provided a low index buffer layer is present to separate high index substrates from the waveguide medium. Polyurethane's index of 1.55 at 6328A compares well with SiO_2's index of 1.45. GaAs, $LiNbO_3$, or other substrates with sputtered or chemical-vapor deposited SiO_2 films are acceptable configurations.

The acutal fan-out array pattern, as shown in Fig. 8-b, is computer generated. Program data includes center-to-center spacing and width of the channel waveguides at the input and output ends of the array, and the length of the array. The computer then generates the pattern on a flat bed plotter.

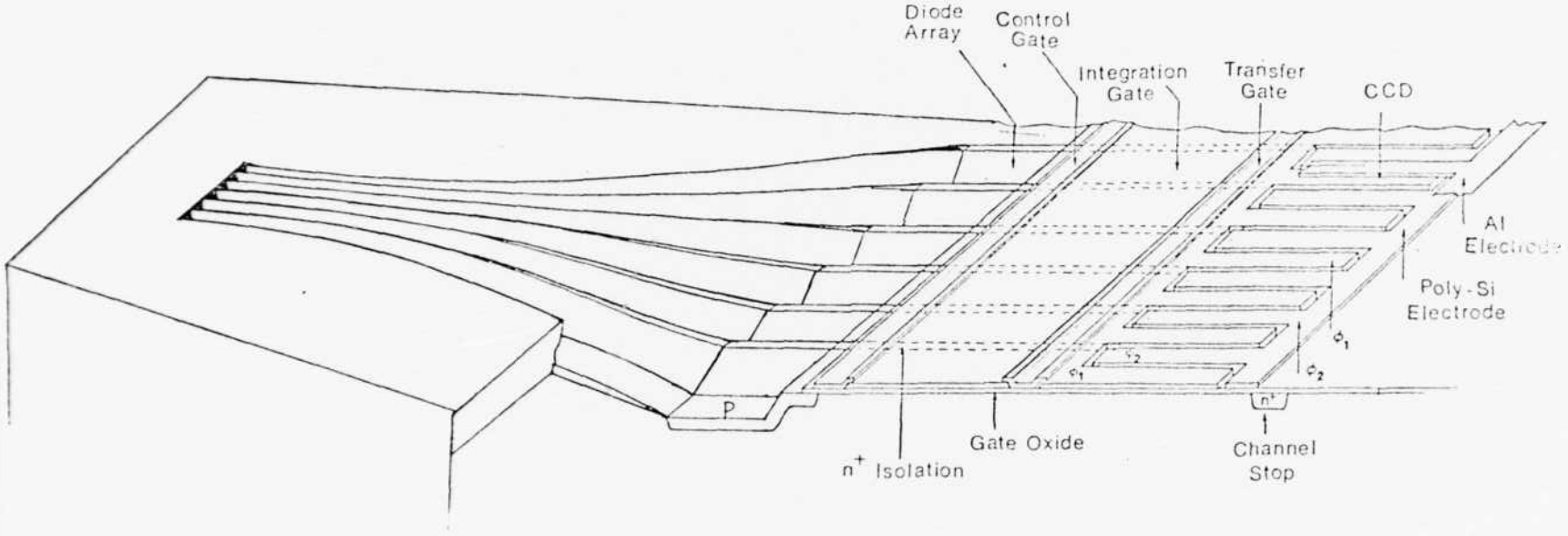

Fig. 8(a) Integrated channel waveguide array-CCD device configuration with channel waveguide array fan-out pattern.

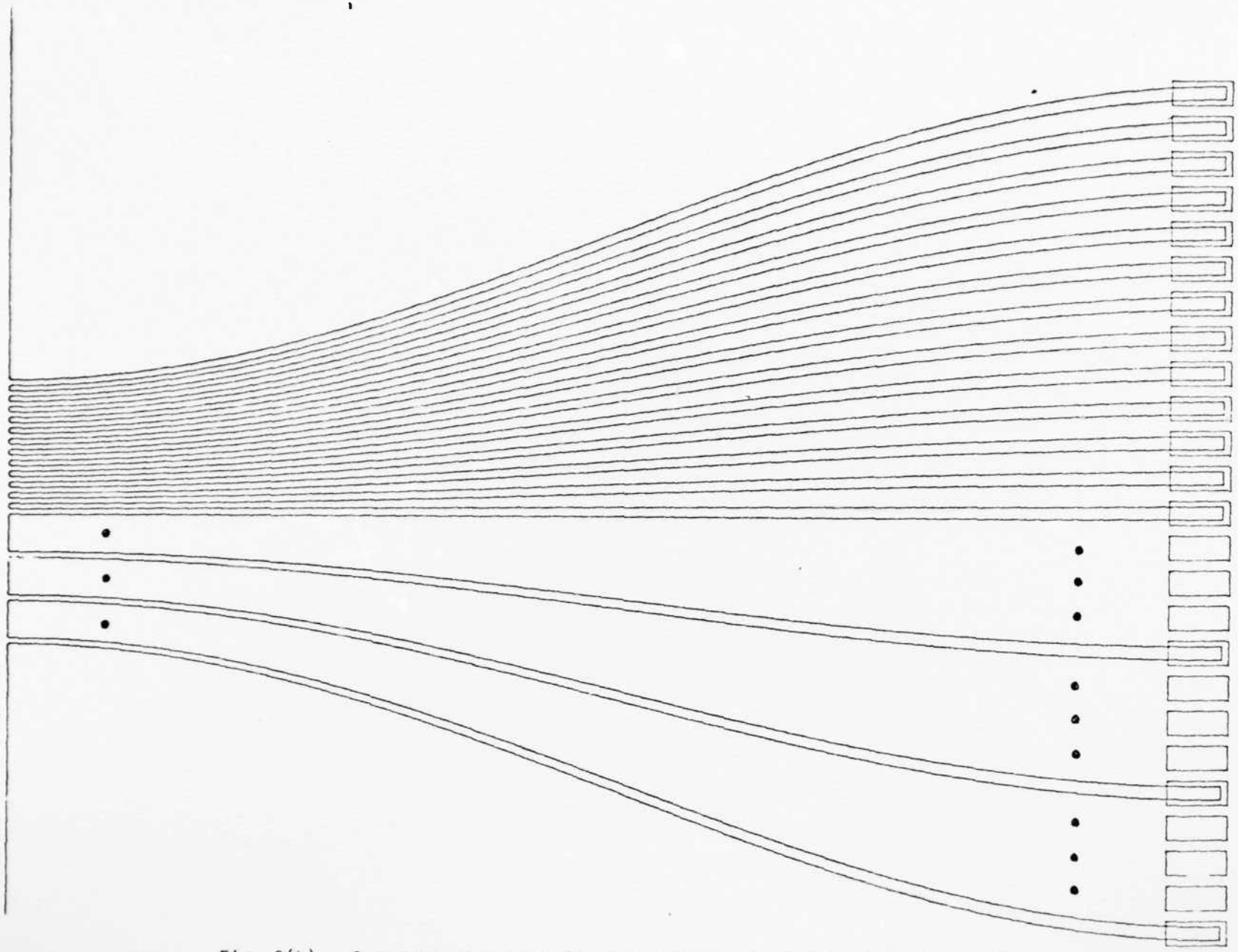

Fig. 8(b) Computer generated fan-out pattern coupled to detectors. For clarity verticle axis is 2X, and only every fourth guide is shown in lower half.

The width of each channel increases linearly between the input and output ends. As each channel follows a sinusoidal path between input and output, the spacing between guides gradually increases. The sinusoidal path is a half cycle in length so that the slope is zero at each end. This is to insure a straight waveguide for best sampling at the input, and alignment ease at the ouptput. Although it was not necessary here, actual straight segments can easily be added to the input and output channel waveguides by the computer, without changing the basic nature of the device.

Waveguide curvature loss is known to increase markedly when the radius of curvature falls below a critical value. Marcuse[32] and Marcatili have studied this problem with Marcatili's model more accurately resembling integrated optical curved waveguides. However, Marcuse's results are simpler to apply to the patterns discussed herein, and Marcuse maintains that agreement is good between his results and Marcatili's.

Following Marcuse,[32] a critical radius of a curvature, R_{crit}, exists in which for a radius less than this, severe scattering will occur, but for a larger radius negligible scattering occurs. In terms of waveguide parameters, R_{crit} is given as

$$R_{crit} = 3n_2^2 d/(n_2^2-n_1^2) \qquad (1)$$

where $n_2 = 1.55$ is the waveguide material refractive index, n_1 is the cladding refractive index equal to 1.0 for air for this case, and d is the waveguide width of the channel waveguide. For a waveguide width of d=5 μm, R_{crit} = 25.695 μm. The minimum radius of curvature for the present device is given as

$$R_{min} = (1+{}^{dy}/_{dx})^{3/2}/({}^{d^2y}/_{dx^2}) \text{ min} \qquad (2)$$

where y describes the sinusoidal path the channel waveguide boundary follows as a function of x. The radius is to be evaluated at the point of maximum curvature, i.e., minimum radius.

As shown in Fig. 8-b, each channel follows a sinusoidal path between evenly spaced input and output array locations. The computer program automatically adjusts the simple equation to achieve proper spacing and alignment. The maximum curvature, minimum radius, occurs for the two outer channels at the extremes in Fig. 8-b. The maximum curvature will occur at the beginning and end points of the array. Dropping the constant terms, the top channel path is described by

$$y = 137.16 \cos \frac{2\pi x}{4572.0} \quad \mu m \tag{3}$$

Then $R_{min} = 3.9 \times 10^3$ μm. From comparing R_{crit} and R_{min}, we conclude that scattering loss due to waveguide curvature should be negligible.

This present device uses channel waveguides formed utilizing polyurethane. This and other polymers have been shown to form optical waveguides having very low scattering and attenuation losses. Ulrich and Weber[34] discussed the properties of a variety of solution deposited waveguide materials, and reported on a thin-film ring laser using polyurethane on a glass rod.[35] Further articles, notably by Swalen, et al.[36] and Tsang, et al.[20] have explored polymer thin films and preferential etching for waveguide fabrication. The fabrication process has been presented by us in the open literature and thus will not be repeated here.[31] Details concerning the CCD-fan-out array device shown in Fig. 8-a have been present by us elsewhere and also will not be repeated here.[4]

D. Optical Cross Talk in Linear Imaging Arrays

An analysis of cross talk in photodetector arrays has been completed

as a part of this AFOSR program.[5] This analysis incorporates effects of carrier diffusion the diffraction spread of an incident ligh beam, and the f/number of the lens focusing the light onto the photodetector array. The analysis is sufficiently general to consider either MOS or photodiode sensing elements.

This analysis complements the experimental development of the fan-out channel waveguide array described in the previous section. A simulation computer program has been developed to predict crosstalk in integrated detector arrays. This simulation effort has been based on an accurate theoretical foundation. The overall system has been divided into sub-systems to aid theoretical analysis and digital simulation. As our work has been oriented towards integrated optical signal processing devices, the simulation starts by determining an accurate field function for the output spot of the lens. This is done using the well known Fourier Transform properties of a convex lens. The original contribution of this effort is the simulation of the substrate processes as shown in Figure 9. Sub-systems for the optical diffraction field and the crosstalk carrier diffusion permit simpler analysis.

In this context it is not practical to discuss all the theoretical and practical details of the simulation. However, an examination of Figure 9 indicates the major features. The optical field in the semiconductor substrate must account for diffraction due to the narrow aperture and for the complex attenuation and phase shift processes which occur in this lossy medium. Near-field simulation of the aperture problem requires careful application of Ketteler's Equations to solve the lossy medium angle dependent wave propagation parameters and use of the Fourier Transform to equate the aperture field with a specturm of plane waves propagating at different angles. An

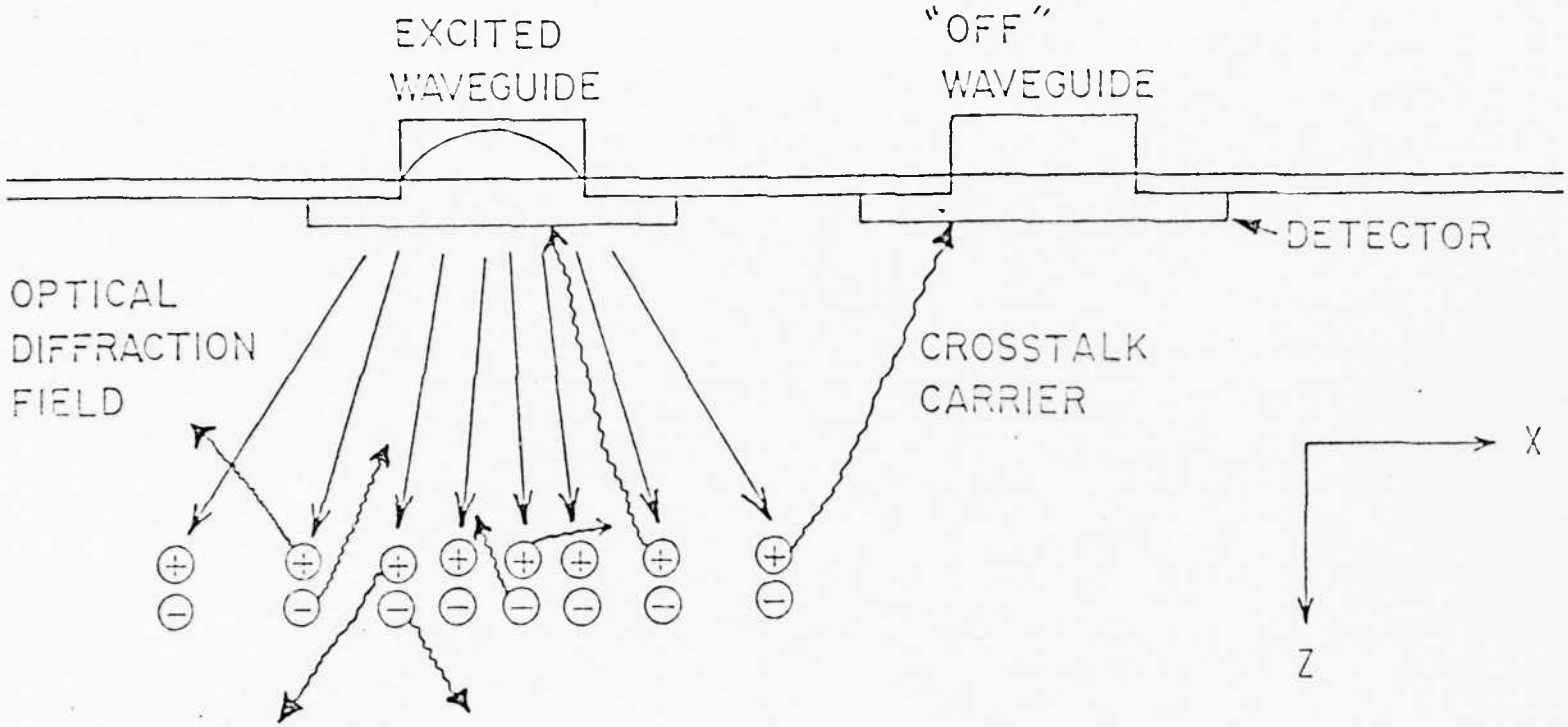

Fig. 9 Photodetector array crosstalk model.

efficient FFT is used to achieve the Fourier Transform, and the different components of the diffraction field have been interrelated so that one spectrum eventually describes three required components. The aperture problem is considered complete when the spatial distribution of photogenerated minority carriers is derived from the Poynting vector of the optical field.

Given the generation rate for minority carriers, the carrier diffusion simulation commences. As shown in Figure 9, it is necessary to determine the ratio of carriers which by random diffusion reach a detector element in the array, resulting in an output current. Carriers which recombine or reach the surface in a non-detector location do not contribute to the output. The diffusion solution can be obtained using an impulse function and convolution summation approach. However, it is computationally more efficient to use the FFT and frequency domain multiplication instead. Further details of the simulation have been published elsewhere.[4,38]

Results of the simulation are briefly summarized in Figure 10. The full extent of possible design variations which can be simulated are too vast to consider here. We present these results to demonstrate the power and utility of the simulation and to verify the fan-out array concept advantages in focal plane line imaging. The figure is a plot of total crosstalk for imaging array systems versus the effective detector element spacing. This effective spacing refers either to actual elements or to input channel spacings of a fan-out array. The three fan-out array simulations use a constant detector array employing 35 micron center spacing. A fourth fan-out ratio would be 1:1. The better crosstalk performance of the fan-out array system over the range of spacings is evident and expected. Simulation of the two systems will simplify the optimal design efforts of fan-out and imaging arrays.

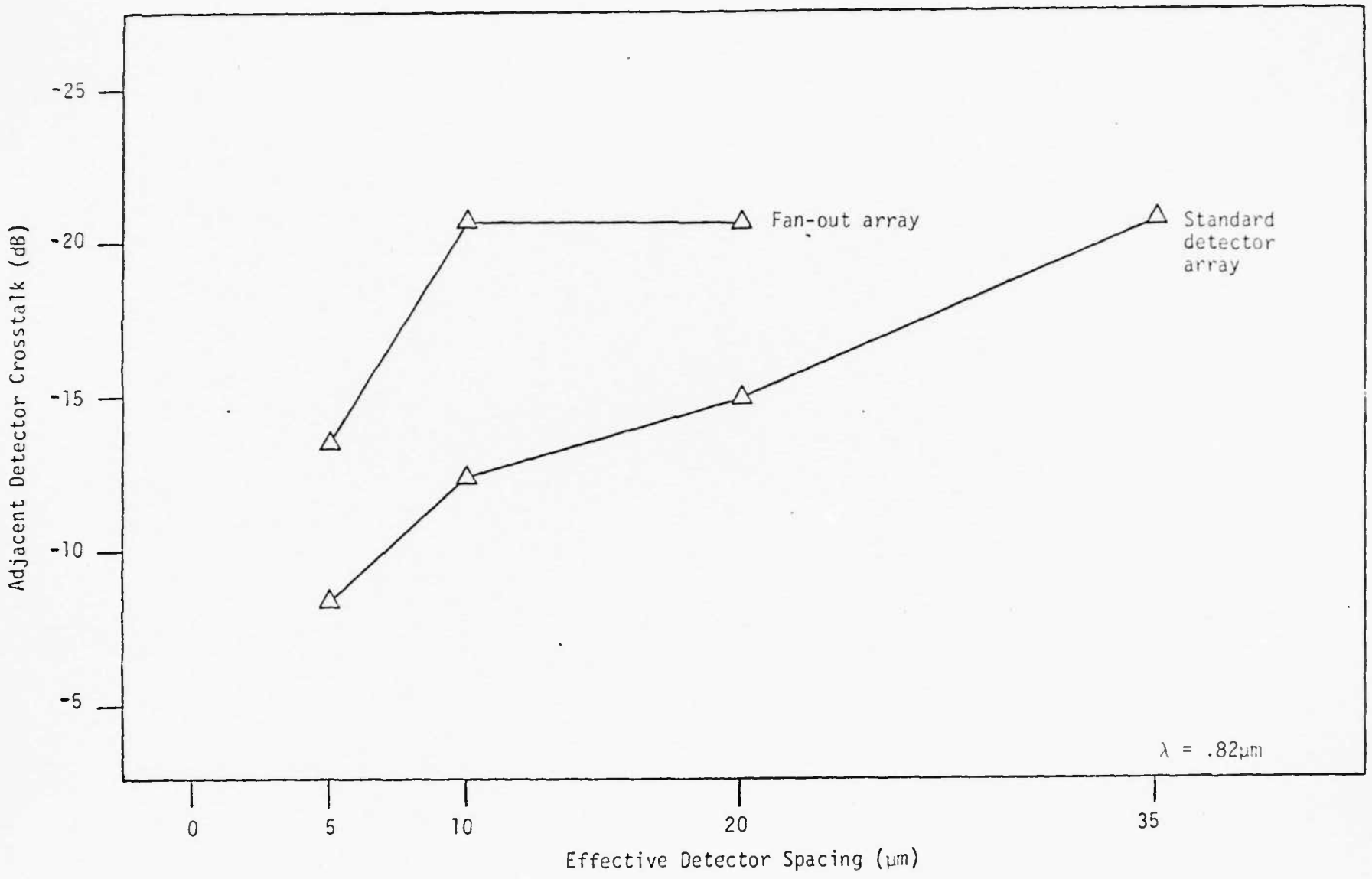

Fig. 10 Plot of adjacent detector element crosstalk in dB as a function of detector element spacing for both a conventional linear imaging array and a linear imaging array incorporating a fan-out array.

The results shown in Figure 10 are the first such quantitative simulations reported on imaging array crosstalk. The number of factors considered in the simulation and the complexity of the processes shown in Figure 9, and others not shown, prevent any accurate closed form solution to this problem. Included in the simulation are parameters for: lens focal length and diameter; free space wavelength; gaussian input beam standard devation; waveguide layer refractive index; detector element spacing, aperture width, and actual element width; diffusion constant; minority carrier lifetime; fan-out array input channel width and spacing; and complex permittivity of the semiconductor substrate. All these may be varied to simulate crosstalk of different systems in a theoretically sound quantitative manner.

E. CCD Examination Using Voltage Contrast With a SEM

The scanning electron microscope (SEM) has been widely used for the examination of various aspects of semiconductor devices and integrated circuits. The voltage contrast mode has allowed imaging of depletion regions on wafer surfaces and on lapped cross-sectional surfaces. In the study carried out under the present AFOSR program we have considered imaging depletion regions in charge-coupled devices which contain double-level metal-oxide-semiconductor (MOS) capacitors with polycrystalline silicon (polysilicon) gates, pn junctions, floating diffusions, and MOS transistors. Of particular note is the observation of transient effects. By applying a low-duty cycle pulse train to a device under SEM observation, we observed transient charging through capacitive coupling of a floating diffusion region.

Besides considering a more complicated device than did a previous study,[37] we also present a new technique for accomplishing breakage of a wafer along a desired line defined on the water surface. This technique results in a very

smooth cross sectional view of the wafer at the desired location. The capability of controlling the position of breakage allows cross sectioning to be implemented so as to intersect the particular device to be examined. This implies that the present SEM technique could be applied to devices contained in actual integrated circuits.

Previously most studies of the cross-section of wafers involved the cutting or fracture of the sample and polishing with successively finer compounds until the desired surface was sufficiently smooth. This results in a smooth surface but the introduction of surface states and contamination to this process is not desirable when attempting to image a charge region. Also, the precise location of the breakage cannot be accurately defined. In the present study we have used the presence of a V-groove formed by anisotropic etching of a (100) surface to define the axis along which breakage occurs. These V-grooves are formed away from the devices of interest and thus do not interfere with device operation. The need for V-grooves to define fracture axes implies that such axes are then limited to lines parallel to the (110) direction.

The technique of using etched grooves to initiate a fracture plane requires that the grooves extend to the edge of the wafer die. Such V-grooves can be formed on a mask with a photorepeater so that V-grooves extend from one die to the adjacent one. The V-groove fabrication step can readily be added to many existing fabrication processes. The position of the V-grooves can then be varied by simply altering the simple mask used for V-groove fabrication. Upon completion of the fabrication process the wafer is then scribed or cut as usual in the direction perpendicular to the V-groove axis. Pressure on the backside of the wafer along an axis parallel to and in proximity to the V-groove axis cause breakage along the (111) plane forming the V-groove side-

wall to occur. This precise control of the fracture location was found to be quite repeatable.

The voltage contrast mode of SEM operation which images secondary electrons was utilized in this study. Voltage contrast arises from the presence of local electric fields associated with applied potential differences which may reduce or enhance secondary emission. Variations in surface potential along a surface are thus manifested as corresponding contrast variations in the SEM image. We utilized an International Scientific Instrument model M-7 SEM which is equipped for voltage feedthrough capability.

We examined a CCD of the type utilized to form the transversal filter described earlier. This CCD is a 4-phase, double-level polysilicon electrode device fabricated on an n type substrate. Figures 11-a and b present pictures of the cross-sectioned CCD with a voltage of -11.7 volts applied separately to two of the four phases. The effect of applying a voltage to a conductor on an SEM image is to cause the conductor to appear much brighter. In Fig. 11-a we see voltage applied to first level polysilicon electrodes, while in Fig. 11-b we see voltage applied to second level polysilicon electrodes. The voltage applied corresponds to a pulse train having period 10 μ sec. in order to simulate electrode clocking. The bus lines for the other two phases were removed in the cross sectioning. Figures 11-a and b indicate that with voltage applied the polysilicon electrodes give good contrast. A close examination of these micorgraphs reveals a darkening of contrast on the cross-sectioned surface just beneath the biased electrodes. Similar photographs of this same device but with higher magnification are prescribed elsewhere.[17] Results demonstrating SEM observation of transient charging of capacitors are not included here because they have been published elsewhere.[17]

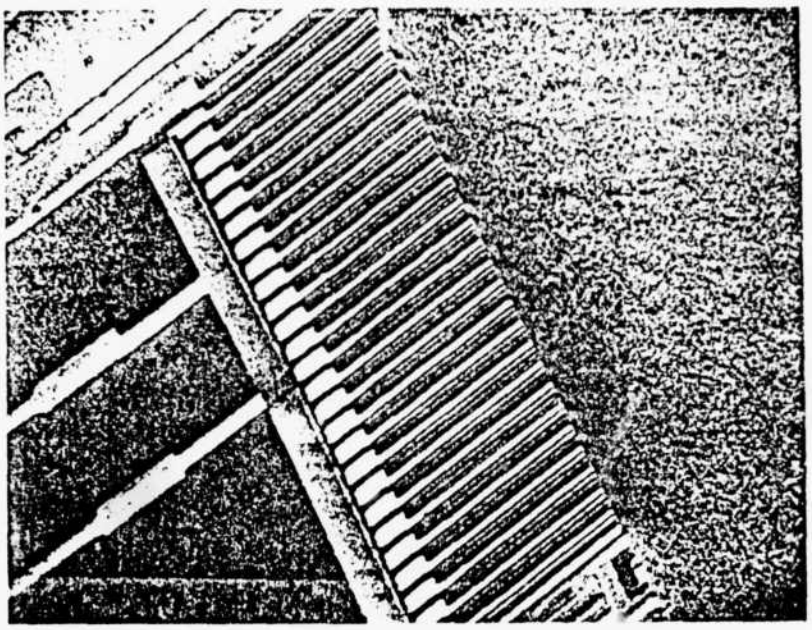

(a)

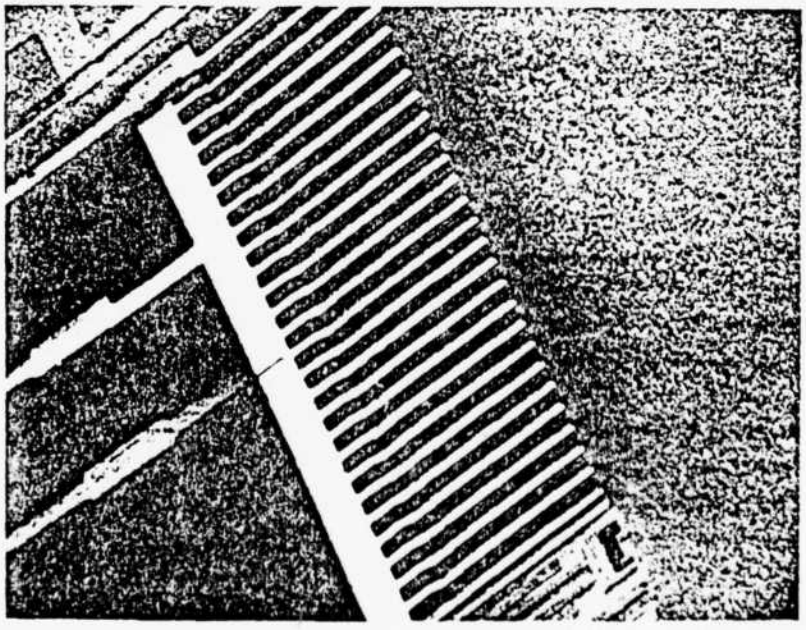

(b)

Fig. 11 a) CCD after cross sectioning with one phase of the first level electrodes biased with a train of pulses having amplitude -11.7 volts, b) Same device in (a) with one phase of the second level electrodes having the same bias applied as in (a).

In the examination and imaging of the cross-sectioned devices, conditions exist that are not normally present during operation of a complete device. The exposure to atmosphere and contaminants, surface states created by the fracturing, and irradiation by an electron beam introduce varying conditions that may or may not be repeatable, not to mention detrimental to the operation of the device. However, data has been obtained in the present study which indicates that devices may possibly be viewed while under operating conditions. Imaging of the CCD double level electrode structure revealed a region of contrast which could clearly be distinguished under the presence and absence of an applied pulse bias. Application of a pulsed bias to the output gate resulted in charge being stored on the floating p+ diffusion at the output while application of a dc bias did not.

In addition a new technique utilizing anisotropic etching for cross sectioning wafers along a lithographically-defined axis has been presented. This technique is simple, involving controlled fracturing, but yields very smooth cross-sectioned surfaces over long lengths near the original wafer surface. The main limitation to this technique is that it can only be applied to (100) oriented wafers and for axes parallel to the (110) direction.

III. Improvements in Materials For Integrated Optics

A. Laser Annealing to Reduce Scattering

It is advantageous to reduce scattering in optical thin-film waveguides for several reasons. Lower scattering loss implies lower requirements for laser source power, thus allowing higher beam quality semiconductor laser sources to be used. As scattering degrades dynamic range[16] in integrated optical signal processing devices such as the spectrum analyzer,[10-12] better performance can be achieved in these devices if a reduction in scattering can be implemented. This class of devices would then become more competitive with other approaches to performing the signal processing. Also, if scattering in thin-film optical waveguides can be reduced dramatically, then the possiblity of an integrated version of an optical fiber interferometer sensor[39] may become feasible.

We have achieved a significant reduction of scattering in glass thin-film optical waveguides by utilizing the technique of laser annealing.[1,2,40,41] Reduction in attenuation measured in dB/cm by as much as two orders of magnitude has been consistently observed after laser annealing for a number of waveguides. These waveguides were formed on a number of waveguide materials fabricated by a variety of techniques. Details of this work has been published so only a brief summary of results will be presented here.

We used a 50W CO_2 laser for laser annealing along with a beam scanner and a focusing lens having a focal length of 6.4 cm. Different power densities were used for different materials. Scanning occurred horizontally, typically at a rate of 1cm/sec, followed by vertical stepping and repetition of the scanning and stepping in order to anneal reasonable-sized areas. Precise measurements of waveguide loss were performed by sampling a streak of light propagating in a thin-film waveguide with a fiber probe incorporated into a

scanning photometric microscope as a function of distance along the propagation axis. The presence of the microscope allowed precise positioning of the fiber with respect to the waveguide and motorized scanning of the fiber transverse to the propagation axis. Electronic signal averaging during this scan including correction for laser power fluctuations was used to improve the precision of the measurement.

Measured values of scattered intensity for the lowest order TE mode are plotted on a log scale as a function of distance along the propagation axis in Figs. 12 and 13 for a ZnO and a 7059 glass waveguide, respectively. A linear mean square fit of the data also is included in these figures. As the vertical scale is logarithmic, the slopes of these lines correspond directly to waveguide attenuation. The low value of loss for 7059 glass associated with the data in Fig. 12 was obtained by first laser annealing and then applying a 1000 A thick surface coating of titanium-doped SiO_2 by spinning a liquid and furnace hardening.[1] This film has a refractive index approximately equal to that of 7059 glass and thus diminishes the perturbing effect of any irregularities on the 7059 glass surface.

Results demonstrating reduction in optical scattering in Si_3N_4, Ta_2O_5, and Nb_2O_5 thin-film optical waveguides has also been observed.[40] Table I summarizes the lowest loss achieved by laser annealing these materials compared to the loss measured before laser annealing and the best results reported preciously. Also included in Table I are similar data for ZnO and Corning 7059 glass.

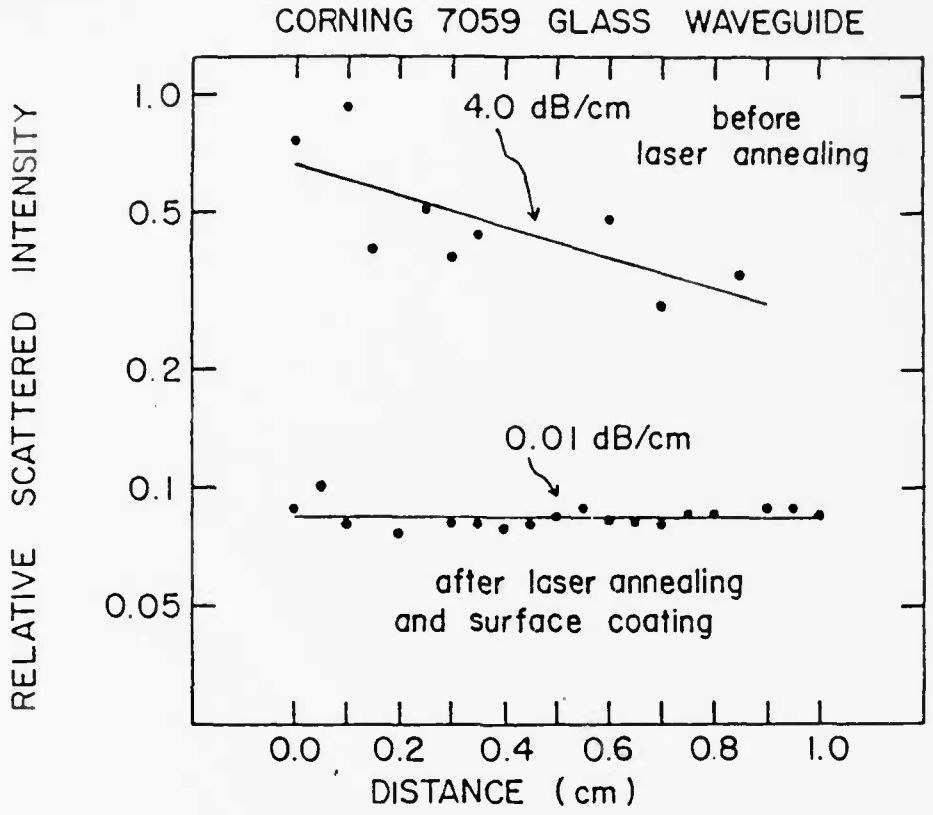

Fig.12 The logarithm of the relative scattered intensity is plotted versus distance along the 7059 glass waveguide. The upper and lower straight lines represent best fits to the data obtained for the TE_0 mode before and after laser annealing, respectively.

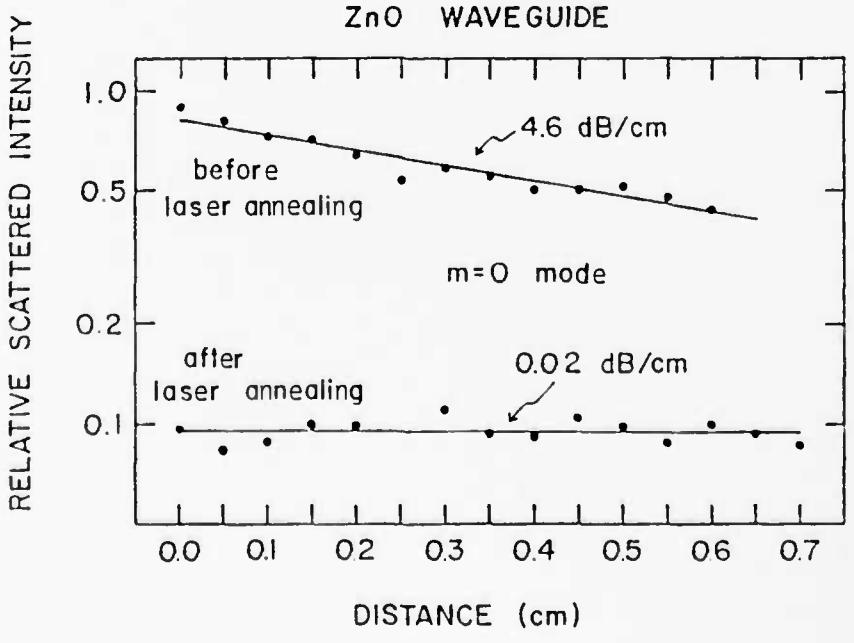

Fig. 13 The logarithm of the relative scattered intensity is plotted versus distance along the ZnO waveguide. The upper and lower straight lines represent best fits to the data obtained for the TE_0 mode before and after laser annealing, respectively.

Table I

WAVEGUIDE LOSS RESULTING FROM LASER ANNEALING
COMPARED TO PREVIOUS RESULTS

Type of Waveguide	Lowest Loss Previously Reported	Current Results Before Laser Annealing	Current Results After Laser Annealing
Corning 7059 Glass	1.0 dB/CM	4.0 dB/CM	0.05 dB/CM (0.01 dB/CM)*
ZnO (Amorphous Substrate)	1.0 dB/CM	2.5 dB/CM	0.01 dB/CM
Nb_2O_5	1.0 dB/CM	7.4 dB/CM	0.6 dB/CM
Ta_2O_5	0.9 dB/CM	1.3 dB/CM	0.4 dB/CM
Si_3N_4	0.1 dB/CM	6.0 dB/CM	0.1 dB/CM

*With Surface Coating Added.

B. *Applications of Phosphosilacate Glass (PSG) Flow to Integrated Optics*

Integrated optical circuits show considerable potential for applications in areas such as signal processing because of anticipated performance levels and economical advantages associated with integrated devices. Some components of the integrated optical devices and of the optical circuits such as geodesic lenses and transition regions to detector arrays require light travelling in a waveguide to cross sharp discontinuites in substrate or isolation layer profiles. The passage of light over a sharp step causes excessive scattering resulting in loss of energy as well as degradation of dynamic range. For a certain type geodesic waveguide lens the guided radiation has to bend through angles as small as 70°. Energy loss considerations dictate that the radius of curvature of the bend be larger than a certain minimum radius R_{crit} which depends on the waveguide parameters. Flow of chemically vapor deposited

phosphosilicate glass is employed to provide smooth tapers for transition regions and bend radii large enough to minimize scattering loss.

In what follows we summarize results published elsewhere[42] concerning the flow behavior of phosphosilicate glass deposited using CVD techniques and flowed under a variety of conditions. Presentation of a theoretical model to account for observed flow characteristics has been deferred pending further investigation. Following a discussion of PSG flow we discuss the formation of PSG bridge structures which span across V-grooves formed in silicon by anisotropic etching. These bridge structures consist of a PSG layer which has been deposited by chemical vapor deposition and then shaped by surface tension during heat treatment. Open space is clearly apparent beneath these bridge structures. The bridge structure has been observed to span V-grooves notches over lengths of 25 mm. Formation of the bridge structures has occurred on a number of samples for several different preparation conditions.

Structures for PSG flow evaluation were prepared by etching V-grooves in 100 type silicon substrates. The grooves were formed by defining rectangular windows in a masking oxide layer and etching the silicon using an anisotropic etchant. The V-grooves thus formed have a notch angle of 70° determined by orientation of the crystal planes. PSG deposited in the notch and heated to a high temperature undergoes flow during which surface tension shapes the glass layer into a smooth bend. Measurement of the radius of curvature of the bend thus provides an indication of the degree of flow.

A standard anisotropic etch using pyrocatechol, ethylene diamine and DI water was employed to etch V-grooves 175 μm deep. The silicon wafers were then thermally oxidized using wet O_2 to grow a silicon dioxide layer approximately 0.75 μm thick.

PSG layers were deposited on the oxidized wafers in a Navtec System 300 rotary hot plate CVD System. A substrate temperature during deposition of

400°C was employed. SiH_4/PH_3 mole ratios of 4, 8, and 14 were used. The O_2/hydride ratio was kept at 12 for all cases. Nitrogen was used as the diluent gas. Total glass flow rates ranged from approximately 1.7 l/min to 2.8 l/min. These conditions were selected to yield values of approximately 5, 8, and 11 mol % P_2O_5 in the glass. Depositions were carried out for periods of 30, 60, 90, 120, and 150 min. We used fixed deposition time periods rather than fixed PSG layer thicknesses because deposition rate varies with deposition conditions and the above procedure simplified work considerably. Lacking continuous monitoring of film thickness, subsequent scanning electron microscope (SEM) examination of cleaved cross sections of the samples was used to determine layer thickness.

Samples were then loaded vertically in furnances for flow at temperatures of 1000°, 1100°, and 1200°V. Ambients during flow were $POCl_3$, dry O_2, and N_2 bubbled through 95°C deionized water. Flow was carried out for 60, 90, and 120 min. The samples were cleaved after flow and and examined in an SEM. Pictures of V-groove notches showing PSG flow were obtained. Radii of curvature of the bends were then measured from these pictures.

Glass flow was carried out in different ambients and at different temperatures. It was observed that if $POCL_3$ was used as the ambient, the PSG layer was damaged by formation of a whitish deposit. Since these layers will form part of waveguide structure surface damage cannot be tolerated as it results in scattering losses. We therefore did not pursue the investigation of this ambient any further.

The results of glass flow at 1200°C for 90 min in various ambients are plotted in Fig. 14. The degree of flow as measured by radius of curvature of the bend is plotted against PSG deposition time rather than layer thickness because data for three P_2O_5 concentrations is shown. The uncertainty in all

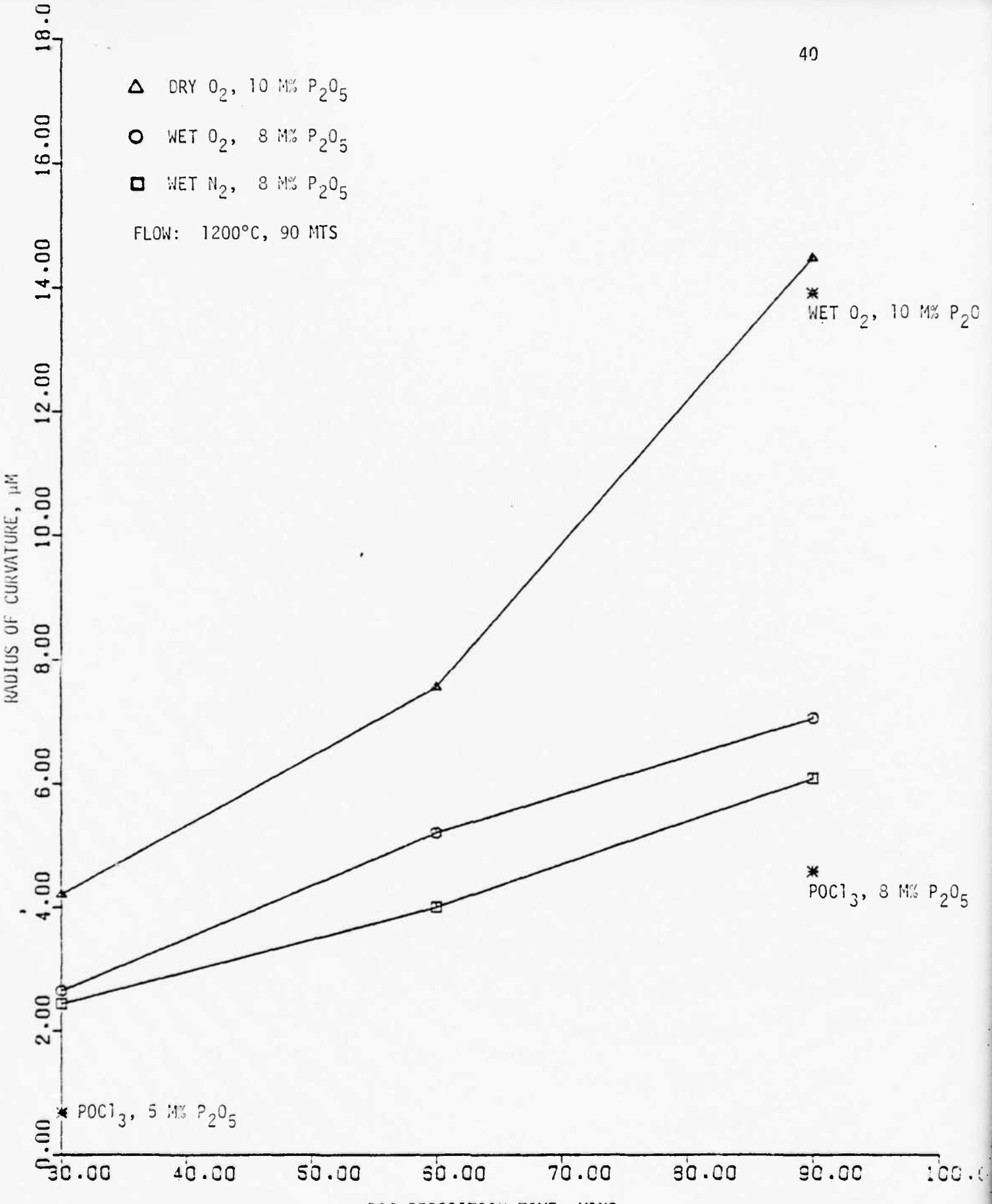

Fig. 14 Plot of radius of curvature of the bend versus PSG deposition time after 90 minutes of flow at 1200°C.

radius measurements is with ±1 μm. This result is typical of a variety of experiments.[42]

It may be concluded that the degree of glass flow is enhanced by increasing (1) phosphorous concentration, (2) flow time, (3) flow temperature, and (4) introducing water vapor in the ambient during the flow process. The degree of flow also increased with increasing layer thickness except in one case. For a wet N_2 ambient the degree of flow seems to have peaked around 14.5 μm. There is little difference between the amount of glass flow in wet O_2 as compared to wet N_2.

Some anomalies were observed and were explained by the presence of a bridge structure spanning the groove with voids beneath the bridges.[43] These voids were formed when the samples were heated to cause PSG glow. Figure 15 shows SEM pictures of these voids. Figures 15(a) and (b) are micrographs of different groove notches from the same sample. It is clearly evident that the presence of a void has increased the radius of curvature of the bend. Figure 15(c) shows another void from a different angle. The bottom of the V-groove notch can be seen easily. Figure 15(d) is an overall view of the coated V-groove after reflow showing bending of PSG at the groove edges. Some of the scatter in data may also be caused by localized variations in glass flow due to inhomogeneous phosphorous distribution. A portion of the scatter may also be attributed to measurement inaccuracies. Sufficient experimentation to determine the statistical properties of this data has not been carried out.

The creation of voids was unexpected since earlier work had not hinted at any such development. Further work remains to be done before the exact conditions necessary for bridge formation are determined. This would involve ascertaining viscosity and surface tension of PSG during flow. Effects of phosphorous diffusion through glass and oxide layers and the substrate with

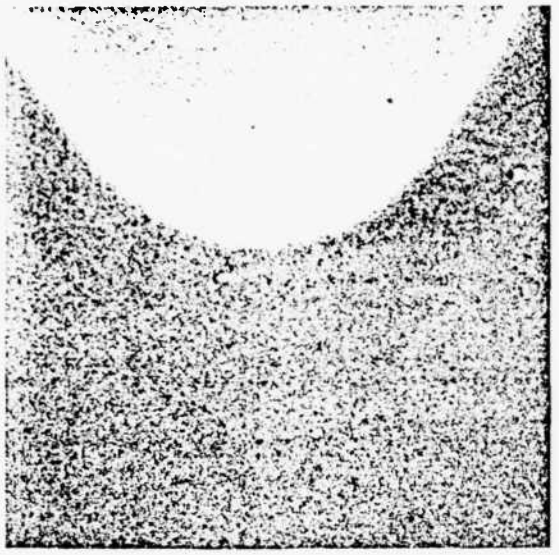

a

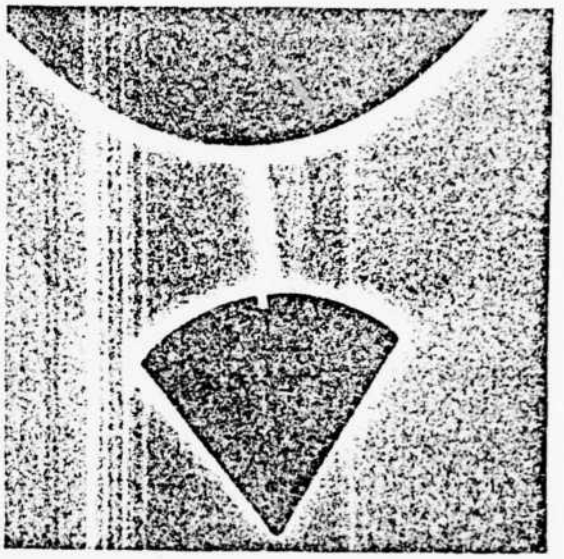

b

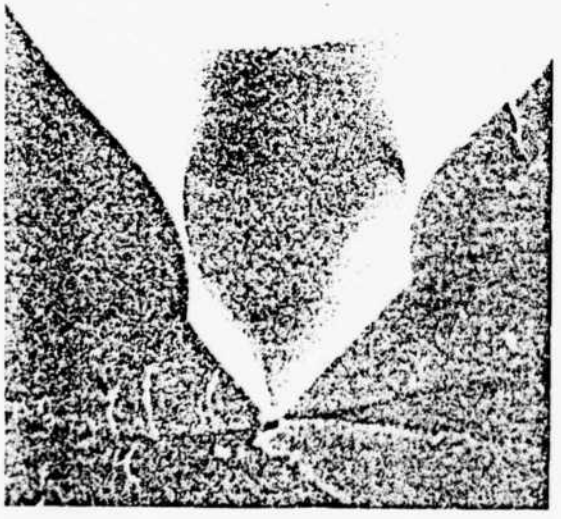

c

d

Fig. 15 a) PSG covered V-groove notch showing formation of a smooth bend due to glass flow. b) Another V-groove notch from the same sample showing increased radius of curvature of the bend due to formation of a void. c) Void formed in PSG deposited in a V-groove notch after glass flow. The bottom of the notch formed by crystal planes can be seen. d) PSG coated V-groove after glass flow.

resulting changes in phase composition need to be taken into account. Thermodynamics of the process plus capillarity effects in the notch also have to be considered. Needless to say this information is also required to develop a complete model of phosphosilicate glass flow under nonvoid forming conditions. It should be mentioned that maximum-sized voids giving rise to maximum bend radii were formed after 90 min in the furnace with a wet O_2 ambient for 22 μm thick layers containing 10 m% P_2O_5.

Finally we found that in the low viscosity regime encountered in some cases, gravitational effects on glass flow can be significant. Since wafers were loaded vertically instead of horizontally with groove lengths parallel to the horizontal plane, the PSG profile after flowing becomes asymmetrical.

C. Use of PSG Flow and Anisotropic Etching to Form a Novel Waveguide Lens

Integrated optical signal processing systems, such as the spectrum analyzer, have considerable potential for application because of anticipated performance levels and the economical advantage associated with an integrated device. Optical waveguide lenses are inherent to the operation of such systems. Implementation of the integrated optical spectrum analyzer is currently being investigated using $LiNbO_3$ instead of a Si substrate, with as noted earlier, $LiNbO_3$ structures providing superior acousto-optic performance, while Si structures allow integration of charge-coupled device image arrays and more economical processing and materials costs. Geodesic optical waveguide lenses are generally used with $LiNBO_3$ structures, while both geodesic and Luneburg lenses have been used with Si structures.[27,28] Fresnel waveguide lenses[29] could possibly be used with either of the above substrates. We report herein the fabrication by anisotropic etching of a geodesic optical waveguide lens utilizing a Si substrate.[44] In comparison to mechanically-formed geodesic

lenses[30] or shadow-sputtered Luneburg lenses,[28] the lens reported herein has the advantages of fabrication simplicity, corrections for aberrations are easily incorporated by altering the curvature of the mask pattern, the substrate area consumed is small, negative lenses can be readily formed, and because the lens position is defined lithographically, its position on the substrate can be accurately controlled with respect to other integrated optical elements.

Previous geodesic optical waveguide lenses have been made by first mechanically forming a depression, which is usually spherical, into the substrate surface, followed by waveguide formation. As light propagating in a waveguide mode enters the depression region, ray components follow geodesic paths having different lengths, thus effecting a lens. We have demonstrated the fabrication of a suitable depression by anisotropic etching. Although the depression formed in this way is not spherical, its shape is controlled by the lithographic pattern, the anisotropic etching properties of the substrate, and the nature of the deposited layers forming the multilayer waveguide structure.

The geodesic lens considered herein utilizes the anisotropic etching properties of (100) surfaces of silicon which allow V-grooves to be formed along (110) directions. V-grooves having various sizes can be formed during a single etching step due to the anisotropic nature of the etching. Since the depth of these V-grooves depends only on the width of the mask opening, by tapering this width, such as in the profile of a thin lens, a variable depth region is created. Fig. 16 illustrates the resulting lens configuration. After forming the variable-depth V-groove, a 1.0 μm layer of SiO_2 is then thermally grown, followed by chemical vapor deposition of phosphosilicate glass (PSG). Reflow of this PSG was then carried out. The glass reflow causes the sharp edges of the V-groove and the bottom of the V-groove to become

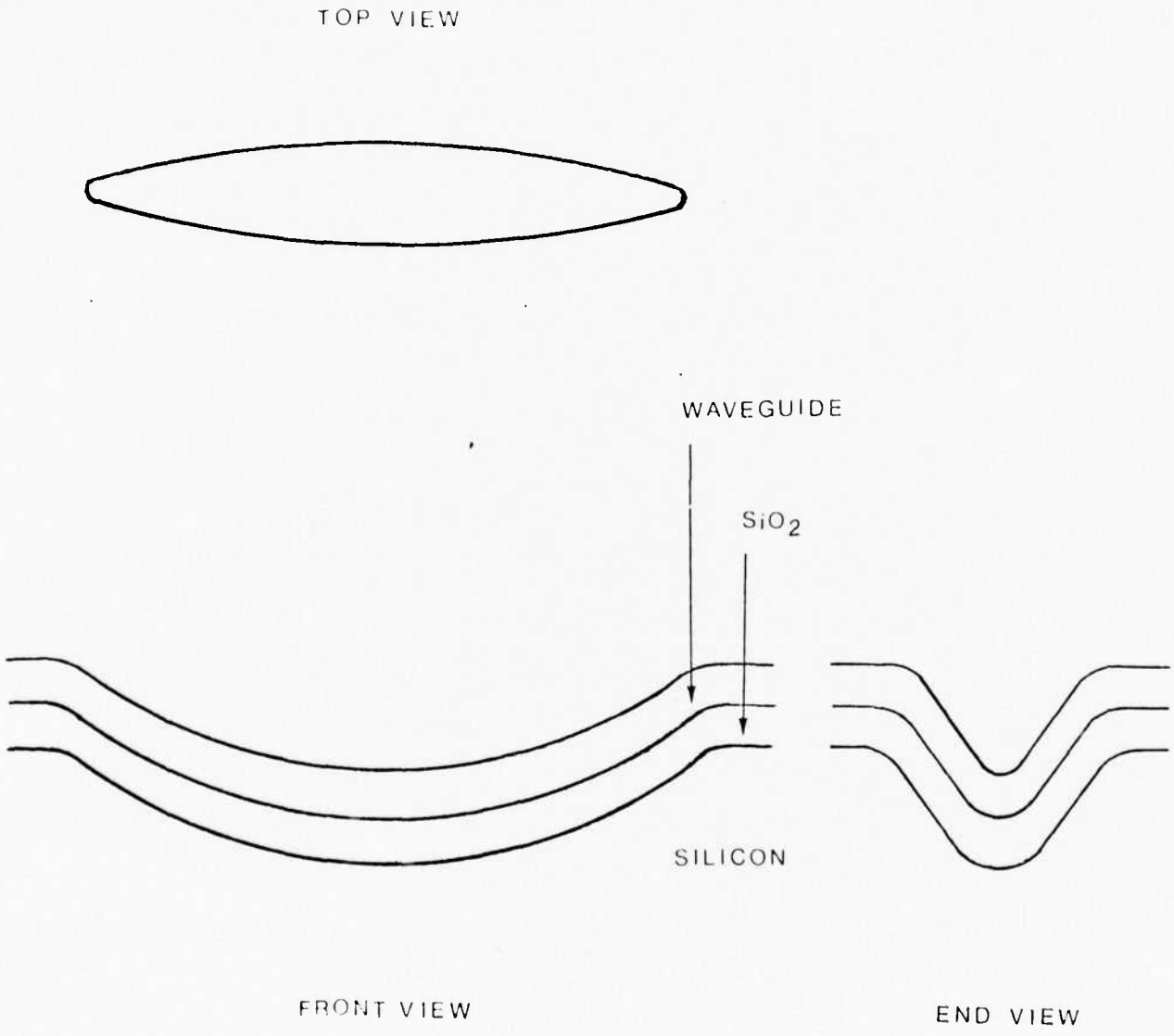

Fig. 16 Configuration of the anisotropically-etched geodesic waveguide lens.

rounded. Repetition of the deposition and reflow process has yielded considerable rounding. The optical waveguide is then formed by depositing a Corning 7059 glass film by RF sputtering. Light propagating in a waveguide mode passes through the waveguide lens with its propagation direction normal to the V-groove axis.

Rounding of the sharp edges surrounding the lens region and along the V-groove axis is necessary in order to minimize optical scattering, as scattering can degrade performance of an integrated optical signal processing system. Considerable rounding has been accomplished by chemical vapor deposition of a 3 μm thick layer of PSG at 400°C. The phosphorous content of the deposited layer is estimated to be 10%. Reflow is then accomplished by placing the wafer in a steam oxidation furnace at 1100°C for 60 minutes. This deposition and reflow was then repeated three times for the samples discussed herein. Rounding could be observed through an optical microscope as an apparent broadening of the bottom edge of the V-groove. After lens fabrication and testing, a sample was fractured along an axis perpendicular to the V-groove axis and examined with a scanning electron microscope. Considerable reflow was evident. The radii of curvature of the reflowed region are R = 68 μm along the lens boundary and R = 11 μm at the bottom of the V-groove. The first of these values exceed the critical value of radius of curvature below which severe scattering would be expected, but the second is slightly below this critical value. Repeating the PSG deposition and reflow steps several more times on future samples may thus eliminate some of the excess scattering occurring in the lens region of the present samples.

Measurement of the lens diffraction pattern was performed for an expanded input beam utilizing reimaging[45], with the result shown in Fig. 17. Instead of utilizing output prism coupling with reimaging, while etching the lens groove we etched a series of lines on each side of the wafer parallel to the

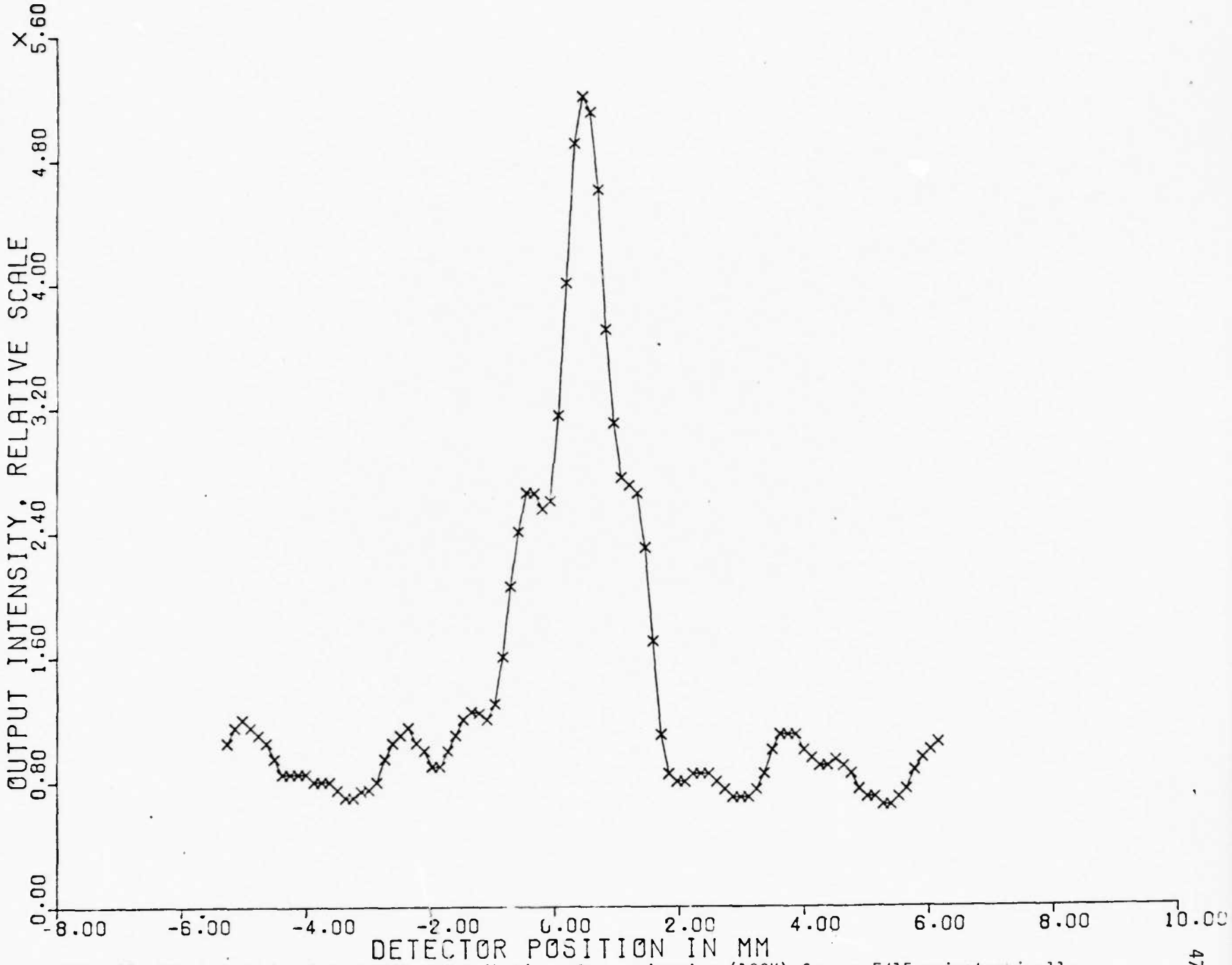

Fig. 17 Measured focal intensity distribution after reimaging (100X) for an F/15 anisotropically

V-groove axis to guide cleavage. Once the position of the focal point was observed, cleavage along the nearest pair of these guide lines was effected. An external cylindrical lens was then slightly adjusted until the focal plane corresponded to the cleaved edge of the wafer. The focal spot was then re-imaged through a microscope to the film plane of the camera attachment. A pin-hole detector combination was then scanned in this plane to obtain a focal spot width that is 1.7X the diffraction-limited value, as shown in Fig. 17.

IV. Planar Waveguides Coupled to Integrated Photodetector Arrays

A. Device Structure

The early portion of this AFOSR research program involved the first demonstration of the integration of a CCD photodetector array with a planar thin-film waveguide. In linear CCD imaging arrays integrated into optical waveguide structures, guided optical waves propagate along the wafer surface entering the imaging device laterally as opposed to from the frontside or backside as in conventional imaging devices. If the waveguiding film is uniform along the direction parallel to the axis of the detector array, a planar waveguide exists and the function of the CCD array is to image light variations in this transverse dimension. Such devices are expected to find applications in integrated optical signal processing structures as they allow conversion of spatial information carried by a guided optical wave in a parallel format to an electrical signal having a serial format.

The configuration of a slab optical waveguide imager is shown in Fig. 18. The dielectric optical waveguide region is located at the left side of this figure. A thin-film dielectric optical waveguide is formed from a material having higher refractive index than the surrounding regions. The presence of the SiO_2 film is necessary as the effective optical waveguide substrate material to prevent significant loss due to evanescent field coupling to the silicon substrate. A very high quality and smooth optical surface of SiO_2 is readily formed by high temperature thermal oxidation. In the region approaching the photodiode array the thickness of SiO_2 is tapered to a smaller value and eventually terminates at the edge of the photodiodes in order to allow the uniform continuation of the waveguide thin film across the photodiodes. The extension of the waveguide thin film along the surface of the photodiodes tends to reduce scattering at the edge of the photodiodes and provide multiple refraction of laser light into the photodiode to increase quantum efficiency.[46]

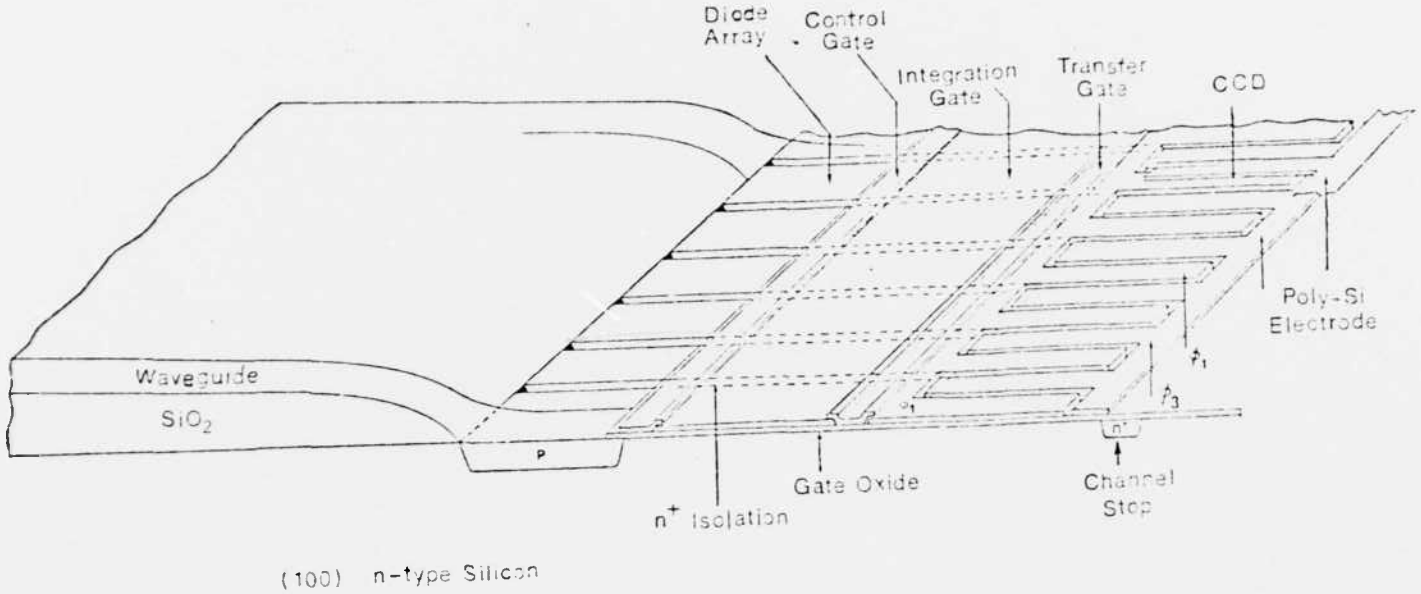

Fig. 18 The later version of a slab optical waveguide imager using V-grooves as isolation between photodiodes, and a four-phase, double polysilicon CCD as analog shift register.

It is important that the taper be gradual, smooth, and uniform along the detector array in order to minimize scattering and preserve signal integrity. Our analysis has shown that scattering near the detector array has more impact in degrading signal processing dynamic range than does scattering from further away.[16] We have successfully fabricated gradual, smooth, and uniform tapers by utilizing carefully controlled undercutting during oxide etching. Details of taper fabrication have been published.[8]

The behavior of the CCDs in these devices are similar to those described previously. Measurements of optical response are included in publications first describing this device.[6,7] One aspect of these CCD's fabricated in this research program which was significantly improved over conventional CCDs was the integrated ouput amplifier. The signal output of a CCD is represented by the magnitude of a charge packet. Conversion of this charge packet into output voltage by current flowing through a load resistor yields voltage magnitudes of only a few tens of mV voltage. Furthermore, not only does this signal appear across the load resistor, but a relatively large clock feed-through voltage is superimposed on the signal. A sample and hold circuit[47] or a differential amplifier can be used to eliminate this clock feedthrough. An output amplifier integrated on the same chip as the CCD which overcomes these disadvantages can also be used. This amplifier is referred to as a gated output amplifier or reset amplifier. Its configuration is shown in Fig. 19-a.[48] This amplifier operates by allowing the charge packet of the CCD output to be transferred to a small gate capacitor of a MOS transistor to obtain a large voltage change. The gated output amplifier shown in Fig. 19-a consists of two MOS transistors and an external load resistor. One is the reset MOS transistor T_1, while the other is the output MOS transistor T_2. The source of the reset transistor is also the output diode of the CCD, and it is

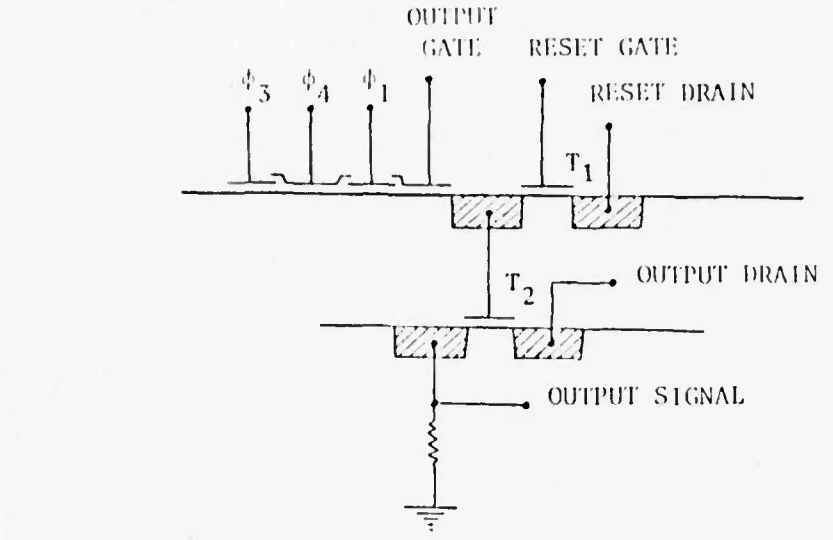

(a)

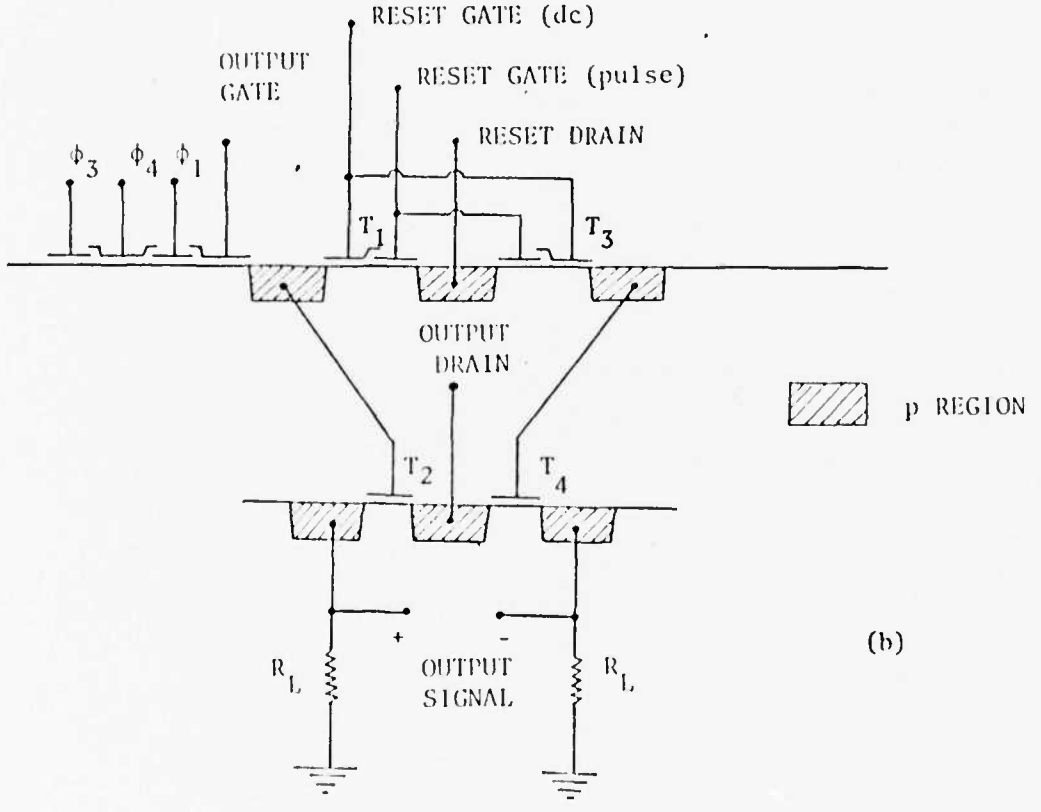

(b)

Fig. 19(a) Conventional gated output amplifier of a CCD having single reset gate.

Fig. 19(b) Dual gated output amplifier of a CCD having an extra dc reset gate.

connected to the gate of the output transistor. The output transistor operates as a source follower. The operation of this gated output amplifier is described as follows. Within each clock cycle, and before signal charge is shifted to the output diode, the reset transistor is turned on for a short period to allow the output diode to be reset to a reference voltage. This reference voltage also sets the gate bias point of the output transistor. After reset is accomplished, the reset transistor is turned off, and the output diffusion is floating. At this time one packet of signal charge of the CCD is shifted into the ouput diode by turning the phase 1 electrode off. The change of voltage V on the gate of the output transistor is proportional to the amount of signal charge Q_s by the relation $V = Q_s/C_e$, where C_e is the gate capacitance in parallel with the p-n junction capacitance. The smaller the capacitance, the larger the output voltage changes. The change of voltage on the gate of the output transistor will correspond to a change of voltage across the load resistor.

Fig. 19-b shows the circuit diagram of the output amplifier used in the four-phase, double polysilicon CCD. A symmetrical dual gated output amplifier with dual reset gates is used. T1 and T2 form one of the gated output amplifiers, and T3 and T4 the other. The amplifier adjacent to the CCD receives signal charge and any clock pick-up from circuit wiring. The other amplifier which has a symmetrical geometric layout receives clock pick-up but no signal charge. The outputs of these two amplifiers are differentially amplified to cancel the clock pick-up. The other feature of this output amplifier is that dual reset gates are used instead of a single reset gate. Use of an extra dc-biased gate can reduce reset clock feedthrough which appears on the output-load resistor. In order to simulate the reset clock feedthrough, the gated

output amplifier has been modeled by utilizing a MOS transistor circuit model stored inside the computer simulation program SCEPTRE.[49] Results of this modeling are published elsewhere.[50]

B. Use in Scattering Measurements

A novel approach to measuring in-plane scattering in thin-film optical waveguides utilizing an integrated photodectector array is presented. The technique is limited to waveguides formed on semiconductor substrates such as Si and GaAs which allow photodiode fabrication. In-plane scattering has been studied previously by focusing a beam of light prism-coupled out of a waveguide onto a plane scanned by a photodetector, as was done by Vahey.[51] The use of integrated detection avoids the use of the output prism which is a significant additional source of light scattering.[51,52] In what follows, we present measurements for a polyurethane thin-film waveguide deposited onto a SiO_2/Si substrate containing a photodiode array. Under certain assumptions, we determine from these measurements the angular distribution of the in-plane scattering and the nature of the surface roughness.

The geometry of the experimental device is depicted in Fig. 20. We used a n-type, two inch diameter silicon wafer on which a 1 μm thick SiO_2 layer is thermally grown. The waveguide film is polyurethane with a thickness of about 1.2 μm. A linear array of photodetectors is formed by an array of p-type diffusions into the substrate. The resulting detectors consist of 100 x 100 μm photodiodes on 125 μm centers. Adjacent to the photodiode array, the SiO_2 is tapered down to the level of the detectors in order to minimize the light scattering that would occur upon waveguide-detector coupling.[32] Electrical connections were made to eight of the detectors.

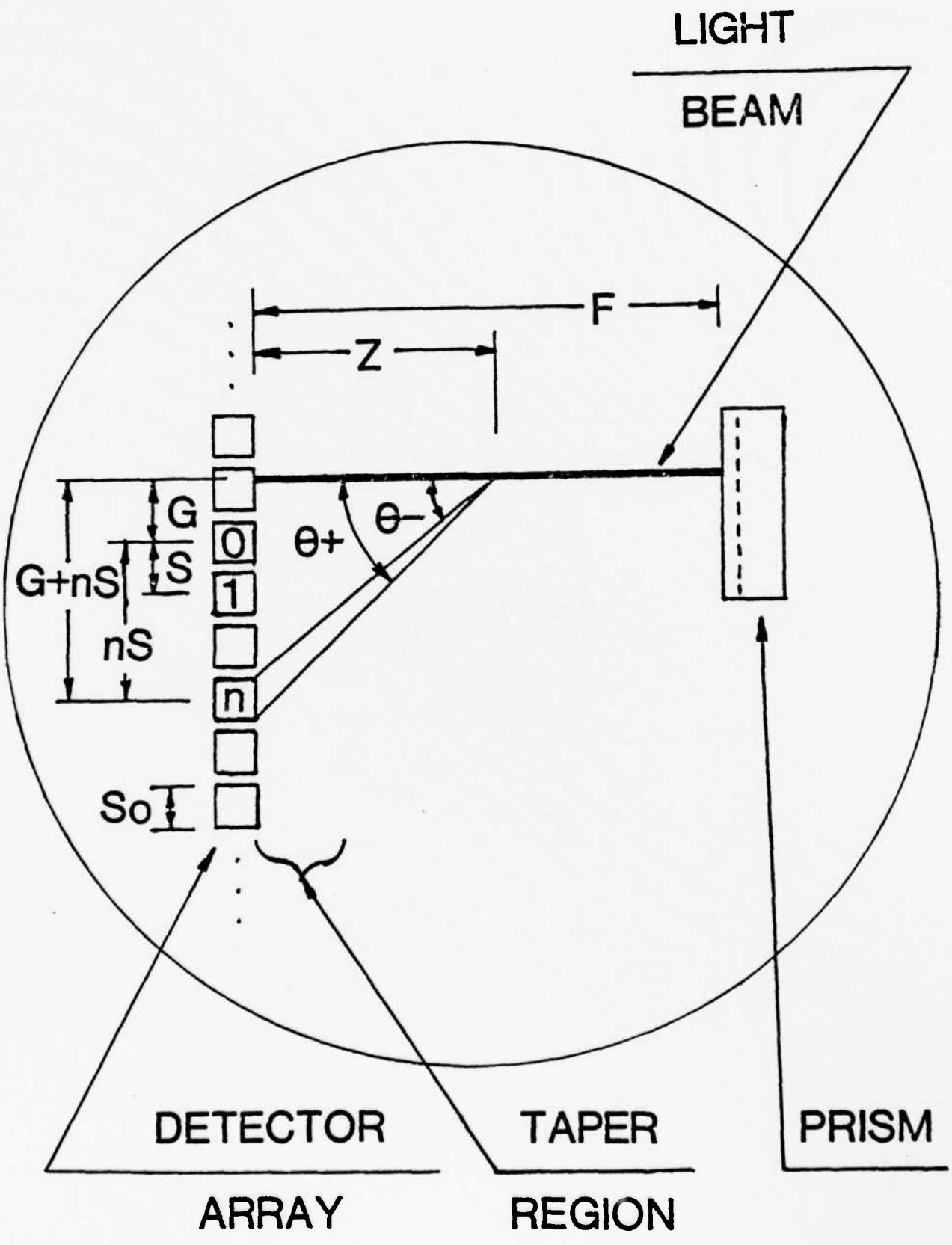

Fig. 20 The geometry of the surface of the experimental device for in-plane scattering measurements.

Light from a He-Ne laser is coupled into the slab waveguide by a glass prism. The light propagates along an axis perpendicular to the photodiode array, as shown in Fig. 20. The relative light intensity scattered into each of the photodiodes along the array is measured by comparing the photodiode currents.

The waveguide for the present experiments was found to have an attenuation of 2.3 db/cm. The scattering measurements are illustrated in Fig. 21. A least squares analysis yields for the in-plane scattering function S the result shown in Fig. 22. The coefficient of determination for the analysis is 96%. The corresponding surface roughness correlation length is 0.16 μm, and the root-mean-square surface roughness is 0.03 μm.

In this section we have thus described an integrated approach to in-plane light scattering measurements in a planar waveguide. Interpretation of the measured data is shown to provide information concerning the nature of the surface roughness causing the scattering. Such information may be useful in characterizing and improving the quality of low loss thin film optical waveguides.

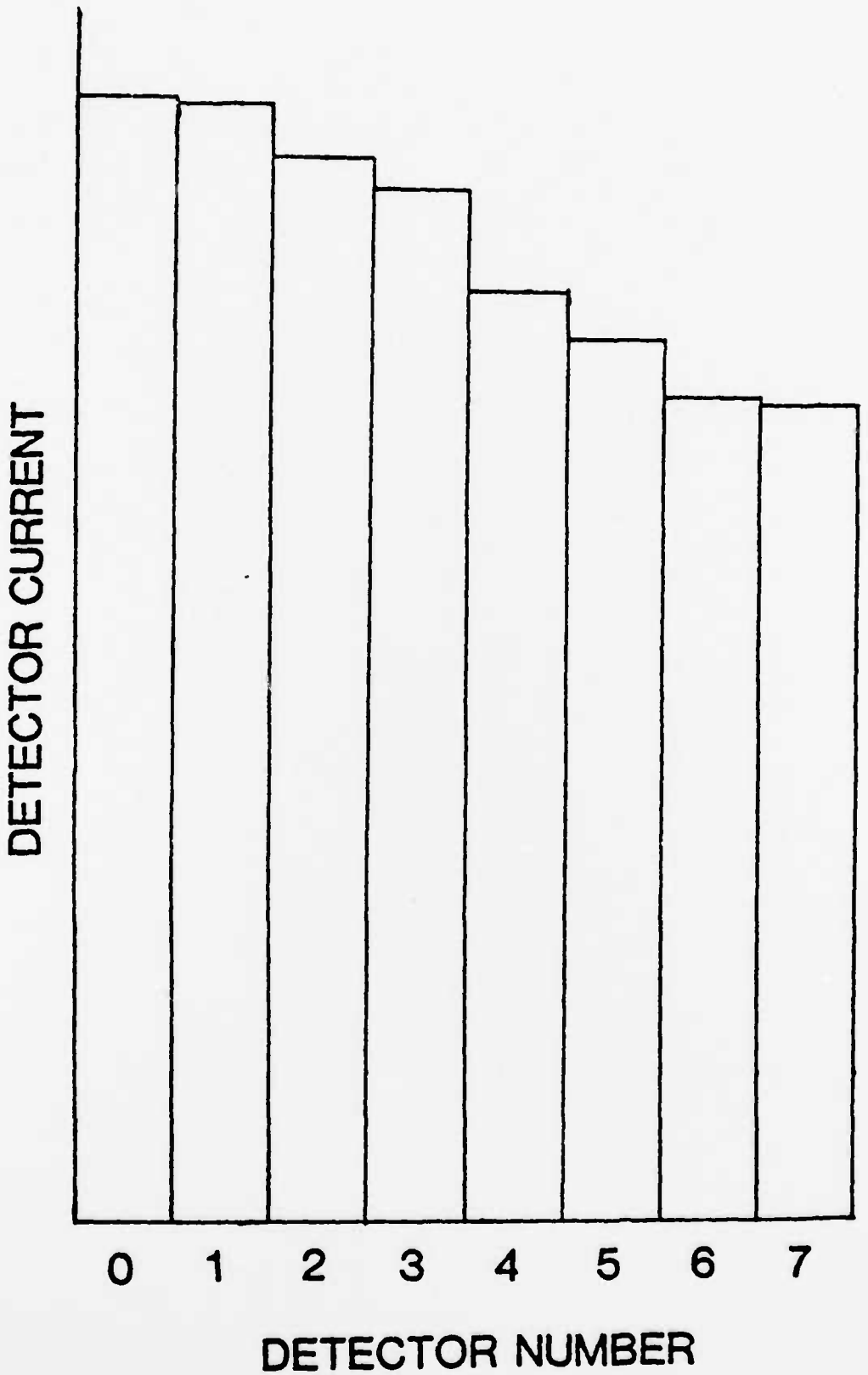

Fig. 21 In-plane scattering measurements of detector current versus detector number for F = 15.7 mm and G = 1.9 mm.

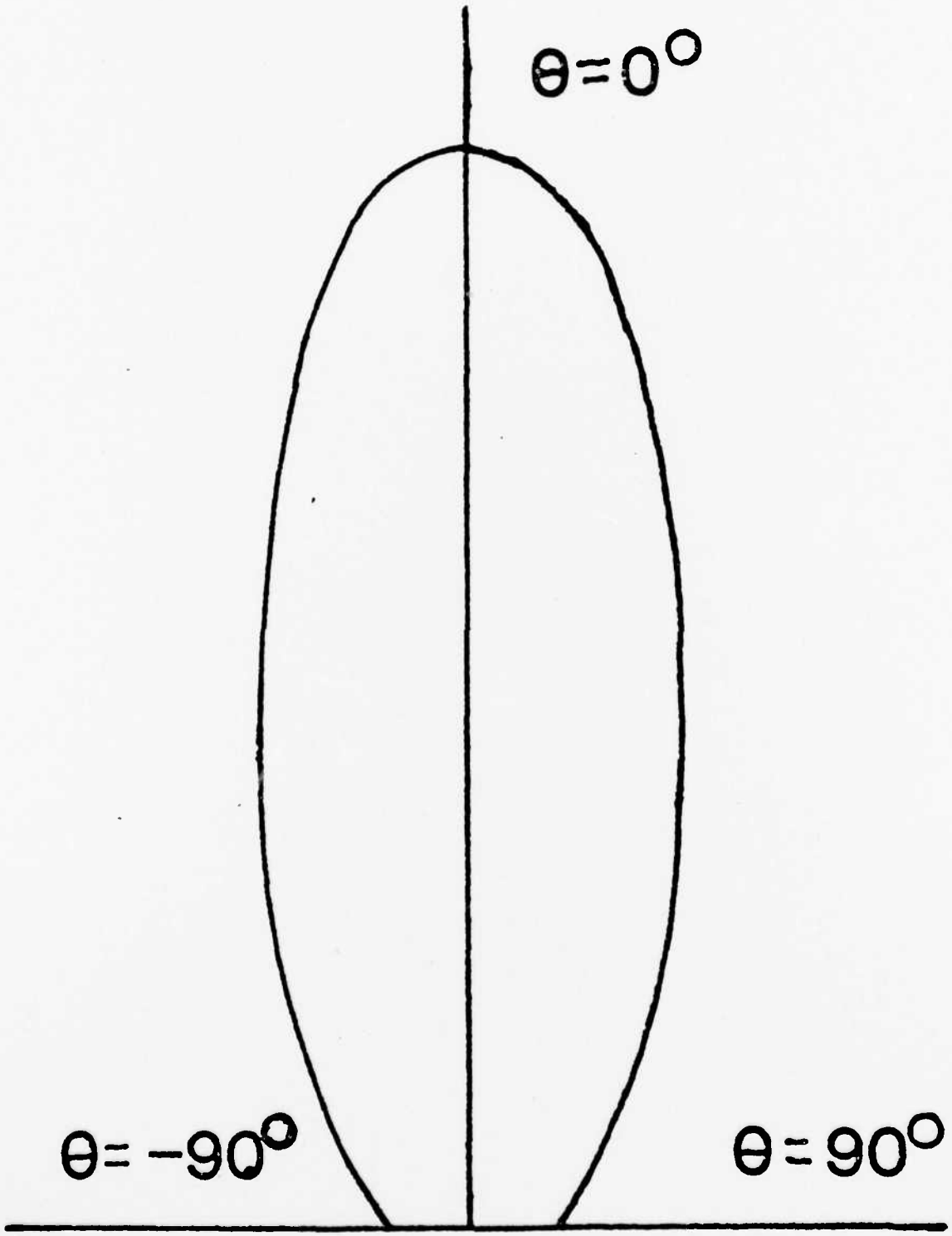

Fig. 22 A polar plot of the angular distribution of the in-plane scattering.

V. Summary and Conclusions

A significant amount of research has been performed as a part of this program sponsored by AFOSR. Most recently, results detained in laser annealing of optical waveguides demonstrate that use of this technique can dramatically reduce scattering in optical waveguides. Dramatic improvement was observed for five materials: Corning 7059 glass, ZnO, Ta_2O_5, Nb_2O_5, and Si_3N_4; while for two of these materials (Corning 7059 glass and ZnO), a value of .01 dB/cm was observed. This value is an order of magnitude better than any value previously reported for any thin film waveguide. The effect of such a reduction in scattering is to allow higher values of dynamic range in integrated optical signal processing and optical communications devices to be obtained, as is shown in analysis performed as a part of this research program. Related to this reduction of scattering, we have also developed a more sensitive technique to measure waveguide scattering loss and a technique to relate the in-plane scattering angular distribution to the mean square surface roughness and roughness correlation length.

As an important part of this AFOSR-sponsored research, surface channel CCDs having transfer inefficiencies as low as 1.0×10^{-4} have been fabricated and integrated with optical waveguides. These devices are 4 phase with two levels of overlapping polycrystalline silicon electrodes. Few universities have reported successful fabrication of CCDs and none of these has reported a better transfer inefficiency. The first published contribution involving CCDs as a part of this AFOSR program reported the integration of a CCD with a planar optical waveguide structure and successful operation. Such a structure could find applications in optical signal processing devices such as guided wave acoustooptic devices. A CCD has also been integrated with an array of channel waveguides with each channel waveguide coupled to a separate linear

image array element. This device is expected to find applications in fiber optical systems as a multiplexer or receiver, in signal processing, and for high resolution imaging. This latter application has been demonstrated with a fan-out channel waveguide array in which the channel waveguide array period is very small at the focal plane. The channel waveguides are then tapered and curved to a larger period at which point they couple to a linear CCD array. This device thus allows high resolution imaging without the necessity of fabricating a very small CCD linear imager. Operation of an integrated optical channel waveguide-CCD transversal filter has also been demonstrated. The presence of optical channels is characterized by many of the advantages that result from the use of optical fibers in various applications.

Notable accomplishements have also been made in several related areas. As a part of our work with CCDs, we performed the first use of voltage contrast in a scanning electron microscope to image CCDs and MOS devices during operation. An analysis of crosstalk in photodetector arrays was carried out which included variations in the imaging lens focal length and diameter, optical wavelength, gaussian input beam standard deviation, waveguide layer refractive index, detector element spacing, aperture width, actual element width, diffusion constant, minority carrier lifetime, and several other parameters. The flow of phosphosilicate glass has been studied and been used with anisotropic etching to form a novel waveguide lens. Near diffraction-limited operation was demonstrated.

VI. List of Program Publications

1. S. Dutta, H.E. Jackson, and J.T. Boyd, "CO_2 Laser Annealing of Si_3N_4, Nb_2O_5, and Ta_2O_5 Thin Film Waveguides to Reduce Optical Scattering," Submitted for publication.

2. F.K. Hopkins, H.E. Jackson, and J.T. Boyd, "In-Plane Scattering Measurements in a Planar Optical Waveguide by an Integrated Technique," Applied Optics, accepted for publication.

3. A. Naumaan, D. Zelmon, and J.T. Boyd, "A thick SiO_2 Graded-Index Planar Waveguide," presented at and published in the Proceedings of the 31st Electronic Components Conference, Atlanta, May 11-13, 1981.

4. J.T. Boyd, S. Dutta, H.E. Jackson, and A. Naumaan, "Reduction of the Effects of Scattering by Laser Annealing of Optical Waveguides and by Use of Integrated Waveguide Detection," Optical Engineering, to be published.

5. S.L. Chen and J.T. Boyd, "Temperature Independent Thin-Film Optical Waveguide," Applied Optics, to be published.

6. J.T. Boyd, S.L. Chen, R.W. Wu, S. Dutta and H.E. Jackson, "Progress in Research on Optical Waveguide Structures Formed on Silicon Substrates," to be presented at and published in the Proceedings of the 1981 National Science Foundation Grantee-User Meeting on Optical Communications, St. Louis, June, 1981.

7. A. Naumaan, R.W. Wu and J.T. Boyd, "Optical Mask Fabrication for Integrated Optical Circuits," presented at and published in the Proceedings of the 31st Electronic Components Conference, Atlanta, May 11-13, 1981.

8. D.A. Ramey and J.T. Boyd, "Computer Simulation of Optical Crosstalk in Linear Imaging Arrays," IEEE Journal of Quantum Electronics, Vol. QE-17, pp. 553-556, 1981.

9. S. Dutta, H.E. Jackson, and J.T. Boyd, "The Use of Laser Annealing and Surface Coating to Fabricate Very Low Loss Thin-Film Glass Waveguides," presented at and published in the Proceedings of the Third International Conference on Integrated Optics and Optical Fiber Communication, San Francisco, April 27-29, 1981.

10 A. Naumaan and J.T. Boyd, "Laser Annealing of Phosphosilicate Glass," Journal of Vacuum Science and Technology, accepted for publication.

11 S. Dutta, H.E. Jackson, and J.T. Boyd, "Extremely Low-Loss Glass Thin Film Optical Waveguides Utilizing Surface Coating and Laser Annealing," Journal of Applied Physics, accepted for publication.

12. J.T. Boyd, S.H. Chang, C.L. Fan, and D.A. Ramey, "Integration of Photodetectors and Optical Guided Wave Structures Formed on Silicon Substrates," presented at and published in the Proceedings of the Society of Photoinstrumentation Engineers Meeting, Los Angeles, February 1981.

13 D.A. Ramey, "Polyurethane Fan-Out Waveguide Arrays and Computer Simulation to Control Crosstalk in Imaging Arrays," Ph.D. Dissertation, University of Cincinnati, 1980.

14. J.T. Boyd, S. Dutta, H.E. Jackson, and A. Naumaan, "Reduction of the Effects of Scattering by Laser Annealing of Optical Waveguides and by Use of Integrated Waveguide Detection," presented at and published in the Proceedings of the Society of Photoinstrumentation Engineers Meeting, Los Angeles, February 1981.

15. A. Naumaan and J.T. Boyd, "Laser Annealing of Phosphosilicate and Borosilicate Glass for Integrated Optics," presented at the 27th National American Vacuum Society Symposium, Detroit, Michigan, 1980.

16. J.T. Boyd, S. Sriram, S.H. Chang, H.E. Jackson, and S. Dutta, "Progress in Research on Integrated Optical Devices Involving Silicon Substrates," presented at and published in the Proceedings of the 1980 National Science Foundaton Grantee-User Meeting on Optical Communications Systems, Cincinnati, Ohio, June 1980.

17. J.K. Rodman and J.T. Boyd, "Examination of CCDs Using Voltage Contrast With A Scanning Electron Microscope," Solid State Electronics, Vol. 23, pp 1029- 1033, 1980.

18. S.H. Chang and J.T. Boyd, "An Integrated Optical Channel Waveguide-CCD Transversal Filter," IEEE Electron Device Letters, Vol. EDL-1, pp 32-34, 1980.

19. A. Naumaan and J.T. Boyd, "Phosphosilicate Glass Bridge Structures," Journal of the Electrochemical Society, Vol. 127, pp 1414-1415, 1980.

20. A. Naumaan and J.T. Boyd, "Phosphosilicate Glass Flow for Integrated Optics," Journal of Vacuum Science and Technology, Vol. 17, pp 529-532, 1980.

21. J.T. Boyd and D.A. Ramey, "Optical Channel Waveguide Arrays Coupled to Integrated Charge-Coupled Devices and their Applications," Optical Engineering, Vol. 19, pp 387-391, 1980.

22. D.A. Ramey and J.T. Boyd, "Polyurethane Fan-Out Channel Waveguide Array for High Resolution Optical Waveguide Imaging," IEEE Trans. on Circuits and Systems, Special Issue on Optical Circuits and Systems, Volume CAS-26, pp 1041-1048, 1979.

23. F.K. Hopkins, "An Integrated Approach to Transverse, In-Plane Light Scattering Measurements in a Slab Waveguide," MS Thesis, University of Cincinnati, 1980.

24. J.T. Boyd and D.A. Ramey, "Optical Channel Waveguide Arrays Coupled To Integrated Charge-Coupled Devices and Their Applications," Optical Engineering, Vol. 19, pp 387-391, 1980.

25. J.T. Boyd, "Integration of Optical Guided Wave Structures With Electronic Devices on Silicon Substrates," invited presentation at the American Physical Society Ohio Section Fall Meeting, Columbus, Ohio, 1979.

26. A. Naumaan and J.T. Boyd, "Phosphosilicate Glass Flow for Integrated Optics," Presented at the American Vacuum Society Meeting, New York City, 1979.

27. A. Naumaan, "An Integrated Optical Geodesic Waveguide Lens Fabricated by Anisotropic Etching," MS Thesis, University of Cincinnati, 1979.

28 S.H. Chang and J.T. Boyd, "An Integrated Optical Channel Waveguide-CCD Transversal Filter," M.S. Thesis, University of Cincinnati, 1979.

29. J.T. Boyd, D.A. Ramey, S. Sriram, and S.L. Chen, "Array of Curved and Tapered Channel Optical Waveguides," presented at and published in the Proceedings of the National Science Foundation Grantee-Users Conference on Optical Communications, Pasadena, California, June 1979.

30. J.K. Rodman, "Investigation of Potential Profiles in MOS and CCD Devices Utilizing Applied Voltage Contrast Techniques in a Scanning Electron Microscope," MS Thesis, University of Cincinnati, 1979.

31 J.T. Boyd, D.A. Ramey, and C.L. Fan, "Enhanced Optical Waveguide Focal Plane Resolution Utilizing a Channel Waveguide Fan-Out Array Coupled to an Integrated CCD," presented at and published in the Proceedings of the Fifth International Conference on Charge-Coupled Devices, Edinburgh, Scotland, September 12-14, 1979.

32. A. Naumaan and J.T. Boyd, "A Geodesic Optical Waveguide Lens Fabricated by Anisotropic Etching," Applied Physics Letters, Vol. 35, p 234, 1979.

33. J.T. Boyd and D.A. Ramey, "Optical Channel Waveguide Arrays Coupled to Integrated Charge-Coupled Devices and Their Applications," presented at and published in the Proceedings of the Society of Photoinstrumentation Engineers Meeting, Washington, D.C., April 1979.

34. J.T. Boyd, C.M. Chuang, and C.L. Chen, "Fabrication of Optical Waveguide Taper Couplers Utilizing SiO_2," Applied Optics, Vol. 18, p 506-509, 1979.

35. C.L. Chen, "Charge-Coupled Device (CCD) Optical Waveguide Imager and Applications," Ph.D. Dissertation, 1978.

36. Chang Lee Chen, "An MOS Random Access Array Selector for Analog Applications," M.S. Thesis, 1978.*

37. J.T. Boyd, "Integrated Optoelectronic Silicon Devices for Optical Signal Processing" Optical Engineering, Vol. 18, p 14, 1979.

38. J.T. Boyd, "Integrated Optoelectronic Devices Utilizing Silicon Substrates," presented at and published in the Proceedings of the 1978 National Science Foundation Grantee-Users Conference on Optical Communications, Pittsburgh, PA.

39. J.T. Boyd, "Integrated Optoelectronic Silicon Devices for Optical Signal Processing and Communications," presented at and published in the Proceedings of the Society of Photoinstrumentation Engineers Meeting, Washington, D.C., March, 1978.

40. C.L. Chen and J.T. Boyd, "Parallel Signal Injection in a CCD Using An Integrated Optical Channel Waveguide Array," IEEE Transactions on Electron Devices, Vo. ED-25, p 267, 1978, and IEEE J. Solid State Circuits, Vol. SC-13, pp 193-195, 1978.

41. C.L. Chen and J.T. Boyd, "Channel Waveguide Array Coupled to an Integrated Charge-Coupled Device (CCD)," presented at and published in the Proceedings of the 1978 Topical Meeting on Integrated Optics, Optical Society of America, Salt Lake City, Utah.

42. J.T. Boyd and D.B. Anderson, "Effect of Waveguide Optical Scattering on the Integrated Optical Spectrum Analyzer Dynamic Range," IEEE Journal of Quantum Electronics, Vol. QE-14, pp 437-443, June 1978.

43. J.T. Boyd, "Application of Integrated Optical Waveguide-CCD Image Arrays to the Integrated Optical Spectrum Analyzer," Invited presentation to representatives of the Naval Research Laboratory and the Air Force Avionics Laboratory at a meeting to discuss future directions for Integrated Optics (IO) ecnology relevant to the development of an acousto-optic IO spectrum analyzer for electronic warfare applications.

44. J.T. Boyd, C.L. Chen, S. Sriram, and D.A. Ramey, "Integrated Optical Silicon Devices," National Science Foundation Grantee-Users Conference on Optical Communications, Columbia University, June 1977.

45. J.T. Boyd and C.L. Chen, "Integrated Optical Waveguide and Charge Coupled Device Image Array," IEEE J. Quantum Electron, Vol. QE-13, pp 282, 1977.

46. C.L. Chen and J.T. Boyd, "Linear Charge Coupled Device Detector Array for Imaging Light Propagating in an Integrated Thin-Film Optical Waveguide,: Proceedings of the Conference on Charge Coupled Device Technology and Applications, Washington, pp 120-125, December 1976.

*Chang-Lee Chen and C.L. Chen listed above are two separate individuals.

VII. Acknowledgements

The authors wish to acknowledge contribution from several others not listed as authors, but who contributed to the work describe herein. Specifically, H.E. Jackson participated in the laser annealing research, J.H. Nevin participated in the design and fabrication of the random access photodiode array, J.K. Rodman performed the SEM observation of CCDs, C.L. Fan participated the fabrication of the CCD integrated with a fan-out array of channel waveguides, F.K. Hopkins performed the scattering measurements, S.C.M. Chuang refined the procedure for forming high quality tapers, and S. Gary performed numerous film depositions to assist in fabrication. The technical assistance of J.T. Garrett and R.A. Kirschner in performing a variety of specialized experimental procedures is appreciated.

Suggestions and constructive critisism arising from discussions with the program monitor, Dr. John Neff, are also appreciated.

VIII. References

1. S. Dutta, H.E. Jackson, and J.T. Boyd, "Extremely Low-Loss Glass Thin Film Optical Waveguides Utilizing Surface Coating and Laser Annealing," Journal of Applied Physics, accepted for publication.

2. S. Dutta, H.E. Jackson, J.T. Boyd, F.S. Hickernell and R.L. Davis, "Scattering Loss Reduction in ZnO Optical Waveguides by Laser Annealing," Applied Physics Letters, to be published.

3. S.H. Chang and J.T. Boyd, "An Integrated Optical Channel Waveguide-CCD Transversal Filter," IEEE Electron Device Letters, Vol. EDL-1, pp 32-34, 1980.

4. J.T. Boyd, D.A. Ramey, and C.L. Fan, "Enhanced Optical Waveguide Focal Plane Resolution Utilizing a Channel Waveguide Fan-Out Array Coupled to an Integrated CCD," presented at and published in the Proceedings of the Fifth International Conference on Charge-Coupled Devices, Edinburgh, Scotland, September 12-14, 1979.

5. D.A. Ramey and J.T. Boyd, "Computer Simulation of Optical Crosstalk in Imaging Arrays," IEEE J. Quantum Electronics QE-17, p. 552, 1981.

6. C.L. Chen and J.T. Boyd, "Linear Charge Coupled Device Detector Array for Imaging Light Propagating in an Integrated Thin-Film Optical Waveguide," Proceedings of the Conference on Charge Coupled Device Technology and Applications, Washington, D.C., p. 120, 1976.

7. J.T. Boyd and C.L. Chen, "An Integrated Optical Waveguide and Charge-Coupled Device Image Array," IEEE J. Quantum Electron., Vol. QE-13, p. 282, 1977.

8. J.T. Boyd, C.M. Chuang, and C.L. Chen, "Fabrication of Optical Waveguide Taper Couplers Utilizing SiO_2," Applied Optics, Vol. 18, p 506, 1979.

9. F.K. Hopkins, H.E. Jackson, and J.T. Boyd, "In-Plane Scattering Measurements in a Planar Optical Waveguide by an Integrated Technique," Applied Optics, accepted for publication.

10. M.C. Hamilton and D.A. Willie, "Acousto-Optic Diffraction in Optical Waveguides," Digest of Technical Papers, Optical Society of America Topical Meeting on Integrated Optics, New Orleans, LA, 1974.

11. M.C. Hamilton, D.A. Wille, and W.J. Miceli, "An Integrated Optical RF Spectrum Analyzer," Proc. of the IEEE Ultrasonics Symposium, Annapolis, MD, 1976.

12. D.B. Anderson, J.T. Boyd, M.C. Hamilton, and R.R. August, "An Integrated Optical Approach to the Fourier Transform," IEEE J. Quantum Electronics, Vol. QE-13, p. 275, 1977.

13. M.C. Hamilton, D.A. Willie, and W.J. Miceli, "An Integrated Optical RF Spectrum Analyzer," Optical Engineering, Vol. 16, p. 475, 1977.

14. T.G. Giallorenzi, W.K. Burns, and J. Donovan, " Fiber Optic Sensors," Paper TuC1, Topical Meeting on Integrated and Guided Wave Optics, 1980.

15. J.T. Boyd and S. Sriram, "Optical Coupling from Fibers to Channel Waveguides Formed on Silicon," Applied Optics 17, p. 895, 1978.

16. J.T. Boyd and D.B. Anderson, "Effect of Waveguide Optical Scattering on the Integrated Optical Spectrum Analyzer Dynamic Range," IEEE J. Quantum Electronics, QE-14, p. 437, 1978.

17. J.K. Rodman and J.T. Boyd, "Examination of CCDs Using Voltage Contrast With A Scanning Electron Microscope," Solid State Electronics, Vol. 23, pp 1029- 1033, 1980.

18. C.L. Chen and J.T. Boyd, "Channel Waveguide Array Coupled to an Integrated Charge-Copled Device (CCD)," presented at and published in the Proceedings of the 1978 Topical Meeting on Integrated Optics, Optical Society of America, Salt Lake City, Utah.

19. C.L. Chen and J.T. Boyd, "Parallel Signal Injection in a CCD Using An Integrated Optical Channel Waveguide Array," IEEE Transactions on Electron Devices, Vol. ED-25, p. 267, 1978, and IEEE Journal of Solid State Circuits, Vol. SC-13, p. 193, 1978.

20 W.T. Tsang, C.C. Tseng, and S. Wang, "Optical Waveguides Fabricated by Preferential Etching," Appl. Opt., Vol. 14, pp. 1200-1206, May 1975.

21. J.S. Harper and P.F. Heidrich, "High Density Multichannel Optical Waveguides with Integrated Couplers," Wave Electronics, Vol. 2, pp. 369-377, 1976.

22. M.A. Copeland, D. Roy, J.D.E. Beynon, and F.Y.K. Dea, "An Optical CCD Convoler," IEEE Trans. Electron Devices, Vol. ED-23, p. 152, 1976.

23. R.W. Broderson et al., "Experimental Characterization of Transfer Efficiency in Charge-Coupled Devices," IEEE Trans. Electron Devices, Vol. ED-22, pp. 40-46, 1975.

24. D.F. Barbe, W.D. Baker, and K.L. Davis, "Signal Processing with Charge-Coupled Devices," IEEE Trans. Electron Dev., Vol. ED-25, pp. 108-125, 1978.

25. F.J. Taylor and V. Shenoy, "Programmable CTD Filters Using Pulse Duration Modulation," Proceedings of the IEEE, Vol. 66, pp. 1091-1093, 1978.

26. J.D. Crow, L.D. Comerford, R.A. Loff, M.J. Brady, and J.S. Harper, "GaAs Laser Array Source Package," Optics Letters, Vol. 1, pp. 40-42, 1977.

27. D.B. Anderson, R.L. Davis, J.T. Boyd, and R.R. August, "Comparison of Optical-Waveguide Lens Technologies," IEEE J. Quantum Electronics, Vol. QE-13, p. 275, 1977.

28. S.K. Yao and D.B. Anderson, "Shadow Sputtered Diffraction-Limited Waveguide Luneburg Lenses," Appl. Phys. Lett., Vol. 33, pp. 307-309, 1978.

29. Paul R. Ashley and William S.C. Chang, "Fresnel Lens In A Thin-Film Waveguide," Appl. Phys. Lett., Vol. 33, pp. 490-492, 1978.

30. B. Chen, E. Marom, and R.J. Morrison, "Diffraction-limited geodesic lens for Integrated Optics Circuits," Appl. Phys. Lett., Vol. 33 pp. 511-513, 1978.

31. D.A. Ramey and J.T. Boyd, "Polyurethane Fan-Out Channel Waveguide Array for High Resolution Optical Waveguide Imaging," IEEE Trans. on Circuits and Systems, Special Issue on Optical Circuits and Systems, Volume CAS-26, pp 1041-1048, 1979.

32. Dietrich Marcuse, Light Transmission Optics, Van Nostrand Reinhold Co., New York, 1972.

33. W. Stutius and W. Streifer, "Silicon Nitride Films on Silicon for Optical Waveguides," Appl. Opt., Vol. 16, pp. 3218-3222, 1977.

34. R. Ulrich and H.P. Weber, "Solution-Deposited Thin Films as Passive and Active Light-Guides," Appl. Opt., Vol. 11, pp. 428-434, 1972.

35. H.P. Weber and R. Ulrich, "A Thin-Film Ring Laser," Appl. Phys. Lett., Vol. 19, pp. 38-40, 1971.

36. J.D. Swalen, R. Santo, M. Tacke and J. Fischer, "Properties of Polymeric Thin Films by Integrated Optical Techniques," IBM J. of Res. and Develop., Vol. 21, pp. 168-175, 1977.

37. N.C. McDonald and T.E. Everhart, Appl. Phys. Letters, Vol. 7, p. 267, 1965.

38. D.A. Ramey, "Polyurethane Fan-Out Waveguide Arrays and Computer Simulation to Control Crosstalk in Imaging Arrays," Ph.D. Dissertation, University of Cincinnati, 1980.

39. T.G. Giallorenzi, "An Overview of Micro-Optic Signal Processing Research," Topical Meeting on Integrated and Guided Wave Optics, Salt Lake City, Utah, 1978.

40. S. Dutta, H.E. Jackson, and J.T. Boyd, "CO_2 Laser Annealing of Si_3N_4, Nb_2O_5, and Ta_2O_5 Thin Film Waveguides to Reduce Optical Scattering," submitted for publication.

41. S. Dutta, H.E. Jackson, and J.T. Boyd, "Reduction of Scattering from a Glass Thin-Film Optical Waveguide by CO_2 Laser Annealing," Applied Physics Letters, Vol. 37, pp. 512-514, 1980.

42. A. Naumaan and J.T. Boyd, "Phosphosilicate Glass Flow for Integrated Optics," Journal of Vacuum Science and Technology, Vol. 17, pp 529, 1980.

43. A. Naumaan and J.T. Boyd, "Phosphosilicate Glass Bridge Structures," Journal of the Electrochemical Society, Vol. 127, pp 1414-1415, 1980.

44. A. Naumaan, "An Integrated Optical Geodesic Waveguide Lens Fabricated by Anisotropic Etching," MS Thesis, University of Cincinnati, 1979.

45. C.M. Verber, D.W. Vahey and V.E. Wood, "Focal Properties of Geodesic Waveguide Lenses," Appl. Phys. Letters 28, p. 514, 1976.

46. J.T. Boyd and C.L. Chen, "Integrated Optical Silicon Photodiode Array," Appl. Opt., Vol. 15, pp. 1389-1393, June 1976.

47. C.H. Sequin et al., "Charge-coupled area image sensor using three levels of polysilicon," IEEE Trans. on Electron Devices, Vol. ED-21, pp. 712-720, 1974.

48. W.F. Kosonocky and J.E. Carnes, "Two Phase Charge Coupled Devices with Overlapping Polysilicon and Aluminum Gates," RCA Rev., Vol. 34, pp. 164-202, 1973.

49. J.C. Bowers, "SCEPTRE: A Computer Program For Circuit and System Analysis," Prentice-Hall Co., 1971.

50. C.L. Chen, "Charge-Coupled Device (CCD) Optical Waveguide Imager and Applications," Ph.D Dissertation, University of Cincinnati, 1978.

51. D.W. Vahey, "Optical Scattering Phenomena in $LiNbO_3$ Waveguides," Technical Digest, Topical Meeting on Integrated and Guided-Wave Optics, Optical Society of America, Jan., 1980.

52. M. Gottlieb, G.B. Brandt, and J.J. Conroy, "Out-of-Plane Scattering in Optical Waveguides," IEEE Trans. Circuits and Systems CAS-26, 1029 (1979).

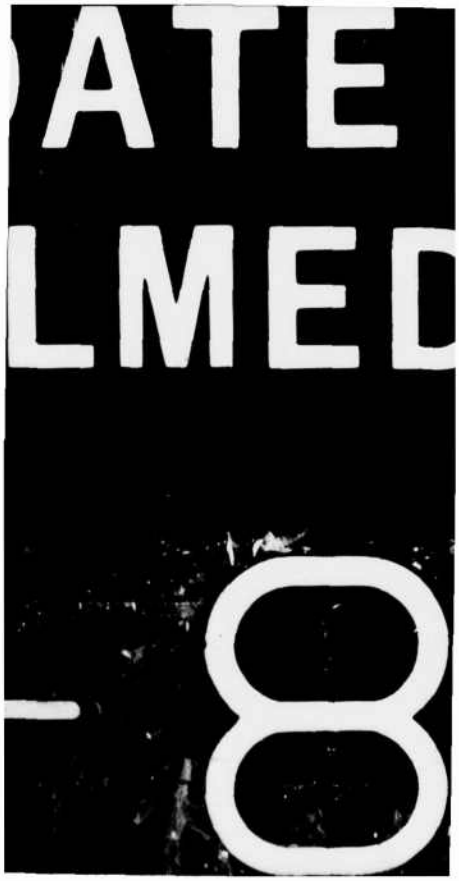
ATE
LMED
8